RSC Advances

PAPER

View Article Online
View Journal | View Issue

Cite this: *RSC Adv.*, 2025, **15**, 23319

Investigation of optical band gap in PEO-based polymer composites doped with green-synthesized metal complexes using various models

Hawkar A. Mohammed,[a] Pshko A. Mohammed *[a] and Shujahadeen B. Aziz *[b]

In this study, PEO-based polymer composites with enhanced optical properties were fabricated by employing a green chemistry approach. A Mn(II) metal complex was synthesized by combining dissolved manganese acetate with an extract of black tea (BT). Then, polymer composite films were prepared using a casting method, incorporating different concentrations of the Mn–polyphenol complex into the PEO matrix. Characterization of the Mn(II) complex was carried out using XRD, FTIR, and UV-vis spectroscopy. The results demonstrated that black tea extract is an effective medium for synthesizing the Mn(II)–polyphenol complex. FTIR analysis confirmed the formation of Mn-PPHNL complexes and their interaction with BT. XRD patterns indicated the amorphous nature of the Mn–polyphenol complex and showed that increasing the complex concentration led to a more amorphous PEO matrix, which was further analyzed using Urbach energy. Additionally, morphological analysis using an optical microscope (OM) image demonstrates that the size of the spherulites attributed to the crystalline phase drastically reduces as the concentration of Mn–polyphenol in a PEO polymer composite increases. UV-vis spectroscopy revealed key optical features, including optical density (n), Urbach energy (E_u), band gap (E_g), and localized state density (N/m^*). Various models, including Tauc's model, absorption edge, ASF, optical dielectric loss, Cody representation and differentiation ($dT/d\lambda$, $dR/d\lambda$, $dn/d\lambda$) approaches, were used to identify the optical band gap of the films. Tauc's plots confirmed the nature of electronic transitions. Dielectric loss measurements indicated a reduction in the PEO bandgap from 5.5 eV to 1.4 eV upon metal complex incorporation. The ASF method further corroborated bandgap changes using only absorbance data. Metallization criteria were applied to classify the polymer's behavior as insulating or metallic. A redshift in absorption edge with increasing complex concentration, from 5.3 eV to 1.42 eV, confirmed the successful interaction between PEO and the metal complex, as validated by UV-vis spectroscopy.

Received 16th March 2025
Accepted 23rd June 2025

DOI: 10.1039/d5ra01881a

rsc.li/rsc-advances

1. Introduction

The aim of materials science research is to develop new materials with tailored properties and to understand the physical and chemical mechanisms underlying these characteristics.[1] Due to their low cost, polymers have been extensively investigated over the past three decades as potential alternatives to metals in a wide range of applications.[2–4] However, polymers generally possess inferior thermal, mechanical, optical, and electrical properties compared to metals and ceramics.[5] Consequently, numerous studies have focused on structural modifications of polymers to achieve desired chemical, physical, and biological functionalities for targeted applications.[3] Polymers exhibit remarkable versatility, making them suitable for diverse applications such as films, coatings, and fiber optics.[6] The incorporation of suitable dopants can substantially enhance and tune the electrical and optical characteristics of polymers.[7–10]

Polymer composites (PCs) typically consist of multiple distinct phases that are physically and chemically integrated on a macroscopic scale and are mutually insoluble.[11] PCs with enhanced optical properties are crucial for a variety of applications, including optical telecommunications, sensors, photovoltaic cells, light-emitting diodes, polarizers, optical waveguides, memory storage, photothermal applications, directional antennas, and biomedical technologies.[12–16] Considerable research has focused on enhancing polymers by incorporating metallic agents, semi-insulators, carbon nanotubes, magnetic nanoparticles, and metal complexes to improve their optical performance.[17,18] Transition metals and other elements in the periodic table's d and f blocks are often referred

[a]*Department of Physics, College of Science, Charmo University, Peshawa Street, Chamchamal 46023, Sulaimanyah, Kurdistan Region, Iraq. E-mail: pshko.mohammed@chu.edu.iq*

[b]*Turning Trash to Treasure Laboratory (TTTL), Research and Development Center, University of Sulaimani, Qlyasan Street, Sulaymaniyah, 46001, Kurdistan Region, Iraq. E-mail: shujahadeenaziz@gmail.com*

to as transition elements. They are categorized as either metals that easily form ions with incomplete d orbitals or metallic elements with unoccupied d orbitals.[19] These metals are further categorized as essential (*e.g.*, Mo, Mn, Cu, Ni, Fe, Zn) or non-essential (*e.g.*, Cd, Ni, As, Hg, Pd).[20] Nevertheless, many conventional methods for processing these metals are complex, energy-intensive, involve low material efficiency, and often require hazardous chemicals.[21] In contrast, green chemistry offers an alternative, where black tea extract serves as a natural chelating agent to replace toxic heavy metal salts, offering an eco-friendly, biocompatible, and cost-effective solution. This approach is entirely environmentally friendly and minimizes health risks for researchers and ecological systems alike.[21–23] It has been shown that amounts of conjugated double bonds, hydroxyl (OH), carboxylic groups, polyphenols, and polyphenol conjugates are primary components of tea leaves.[24,25] Another study also indicates that tea extract mixtures include numerous active functional groups and ligands essential for complexation with heavy metal cations and/or polymers.[26] Due to their biodegradability, nontoxicity, and solubility in water, tea polyphenols are frequently a top choice for reducing and stabilizing agents. Moreover, the molecules in tea extract possess alcoholic functional groups that can be used to stabilize the final product.[27] A published study developed an iron–polyphenol complex using eucalyptus leaf extract solution.[28] The polyphenols can interact with the other metals throughout coordination chemistry. Several studies have shown that the bioremediation method can be used to produce metal complexes or organometallic-based materials that can capture the positive ions of heavy metal salts, such as $CuCl_2$, cobalt(II) acetate, and $SnCl_2$. The studies also demonstrate that coordination compounds exhibit substantial absorption over the visible spectrum.[29–31] Therefore, a black tea extract solution and the green technique were employed in this study to synthesize the manganese metal complex (Mn(II) complex). Polyphenols in black tea leaves interact with the Mn^{+2} cations to synthesize the Mn(II)-complex. The metal complex is then added to polyethylene oxide (PEO) to create polymer composites that show remarkable optical characteristics.

Polyethylene oxide (PEO) is selected as the host polymer due to its biodegradability, biocompatibility, flexibility, and semi-crystalline morphology.[3,32–36] Also, it is a linear polymer, a relatively inexpensive and water-soluble material. Due to PEO being a linear polymer, the uniformity of its structural units allows for a high degree of crystallinity in its pure state.[37,38] Nonetheless, the applications of pure PEO have been limited due to low ionic conductivity, a wide bandgap, and inappropriate refractive index. Consequently, several researchers are presently concentrating on modifying PEO by including metal complexes to enhance its characteristics and mitigate its limitations.[11] However, the PEO is a particularly appropriate choice for application in the field of optics.[39] Polymer composites are mostly being investigated to modify their electrical and optical properties. Improving the electrical and optical characteristics of polymers has lately attracted researchers' attention due to their widespread use in optical systems and their remarkable features of interference, reflection, anti-reflection, and polarization. Moreover, current studies indicate that photonic and optoelectronic device applications require (PCs) characterized by substantial absorption and a low band gap energy (E_g).[31] Previous studies indicated that solutions with black and green tea extracts were crucial for reducing the energy gap of polymers such as PMMA, PVA, and PEO.[22,40,41] It has been shown that metal complexes are most notable for reducing the bandgap for PEO compared to other forms of additives like salt, ceramic nanoparticles NPs, and metal NPs.[19] Caused by the C–O, C–C, and C–H in the PEO,[42] it can interact with the functional group in black tea which creates a coordination compound between metal complexes and PEO, help to reduce bandgap easily compared to other type filler. Substantial studies into the optical properties of polymers employing PEO as the principal host material. Muheddin *et al.* used various concentrations of Zn–polyphenol complex with PEO to reduce the band gap of the polymer from 5.5 to 0.6 eV.[22] Utilizing an analogous approach, Abdullah *et al.* used carbon nanodots (CNDs) and silver nanoparticles (Ag NPs) incorporated into PEO to drop the energy gap from 6.22 to 5.95 eV.[37] Aziz *et al.*[43] developed green chemical methods to fabricate a polymer composites with silver nanoparticles (PEO-Ag), the result show that the bandgap declines from 6.2 to 3.57 eV.[43] This study aims to fabricate environmentally sustainable PEO-based polymer composite embedded with a Mn(II)–polyphenol complex derived from black tea extract and to examine their structural and optical behavior through comprehensive characterization methods. It also improves the absorption of visible light of the fabricated polymer composites. The findings will provide a new domain for research in polymer composite manufacturing, distinct from traditional approaches that use ceramic fillers or metal nanoparticles. Furthermore, the progress of the present study employs an entirely eco-friendly technology for synthesizing metal complexes using sustainable methods. Quantitatively, the findings exhibit that the extract tea solution contains significant polyphenols and ligands capable of complexing with transition metal salts, resulting in the formation of precipitated metal complexes beneficial for the fabrication of polymer composites with reduced bandgap (E_g) from 5.5 to 1.4 eV with increasing Mn(II)–polyphenol complex to a specified proportion that makes it appropriate for applications in optics.

2. Methodology

2.1. Metal complex synthesis

To prepare the black tea extract, 23.68 g of black tea leaf was boiled in 300 mL of distilled water (D.W.) at 90 °C. The resulting mixture was filtered by paper filtration (Whatman paper 41, cat. no. 1441), which has a pore radius of 20 μm, to remove solid residues. Then 20 g of manganese acetate ($Mn(CH_3CO_2)_2 \cdot 2H_2O$) salt [MW = 245.09 g mol^{-1}] was dissolved in 300 mL of distilled water under consistent stirring to obtain a homogeneous solution. Caused by black tea extracts are rich in polyphenols, which contain acidic hydroxy groups (*e.g.*, in catechins like EGCG) capable of deprotonation under physiological conditions, forming negatively charged oxygen atoms attached directly to aromatic groups. These oxygen ions act as Lewis

bases, donating electron pairs to the d-orbitals of transition metal ions (*e.g.*, Mn^{2+}), forming stable coordination complexes. This mechanism is well-documented: polyphenolic structures, particularly *ortho*-dihydroxy groups in galloyl moieties, exhibit strong metal-chelating properties due to their low pK_a (~8–10), enabling deprotonation and subsequent binding *via* lone pairs.[44–46] For instance, EGCG forms stable complexes with Fe^{3+} and Cu^{2+} *via* catechol-O-groups,[47] a principle extendable to manganese ions given analogous d-orbital interactions. This adjustment aligns with established literature on polyphenol–metal coordination chemistry. As a result, the manganese ion and the black tea polyphenol form a coordination bond. All polyphenols have multiple donor sites that can bind to a single manganese ion because they provide electron pairs to manganese ions. Finally, we added manganese acetate to the extracted black tea solution at 80 degrees Celsius and mixed it over 1 hour to create a Coordination compound Mn^{+2}–polyphenol (PPHNL). At the base of the tube, the extract solution's dark tea hue gave way to a brown tint. The observed color transition—from dark tea to lighter brown in the supernatant and dark brown precipitate-stems from Mn(II) complexation with polyphenols in black tea. Polyphenols act as ligands, forming insoluble Mn(II)–polyphenol complexes that settle as a precipitate, while residual soluble complexes or unbound ligands in the supernatant produce a lighter tint. The color shift arises due to ligand field effects: polyphenols induce d-orbital splitting in Mn(II), enabling d–d transitions or ligand-to-metal charge transfer (LMCT), which absorb specific wavelengths (*e.g.*, blue/violet). The complementary color (orange-brown) becomes visible, aligning with the color wheel. The darker precipitate reflects concentrated complexes with intense light absorption, while the supernatant's paler hue corresponds to diluted or smaller soluble species.

Scheme 1 depicts the preparation of the Mn-PPHNL-based material. For the purpose of eliminating anions of the dissolved salt and uncoordinated cations of the zinc, the sediment was kept in the beaker, and any liquid or distilled water that accumulated on top of the black tea sediment was removed with a syringe and replaced with an equivalent amount of distilled water at regular intervals of five days. Distilled water was used to repeatedly rinse the resulting residue.

2.2. Synthesis of polymer composites

Employing the established solution cast procedure, we created a PEO solution [MW = $2 \times 10^{+6}$ g mol^{-1}] and mixed it with the Mn–polyphenol complex to create a polymer composite. First, we prepare the PEO polymer solution by mixing 0.200 L of acetonitrile with 2 g of PEO. We used 0.125 g of glycerol in each beaker until we reached the plasticizer to omit film brittleness after one hour of mixing with a magnetic stirrer. The initial and second identical PEO solutions are then gradually supplemented with ten and twenty mL of the Mn–polyphenol-based material solution in ten-mL increments. For three hours, the mixtures were incessantly stirred until homogeneous solutions were achieved. For pristine specimens and PEOs containing zero, ten and twenty mL of Mn–polyphenol-based material solution, respectively, the samples were labeled as PEOMnMC0, PEOMnMC1, and PEOMnMC2. PEO impregnated with a foreign material, the Mn(II)–polyphenol complex, was used to generate composite films using the solution cast method. The mixture's components were positioned in Petri dishes and allowed to air out dry at ambient temperature. Scheme 2 demonstrates how to create a polymer composite; the water in the glass Petri dishes during the dry process gradually evaporated.

2.3. Spectroscopic investigations

The X-ray patterns of polymer films were recorded using an X-ray diffractometer (ADX 2700) with Cu-Kα radiation (λ = 1.5406 Å). The scan rate was set to 2° min^{-1}, and the Bragg's angle (2θ) was set between 10° and 90°. Fourier-transform

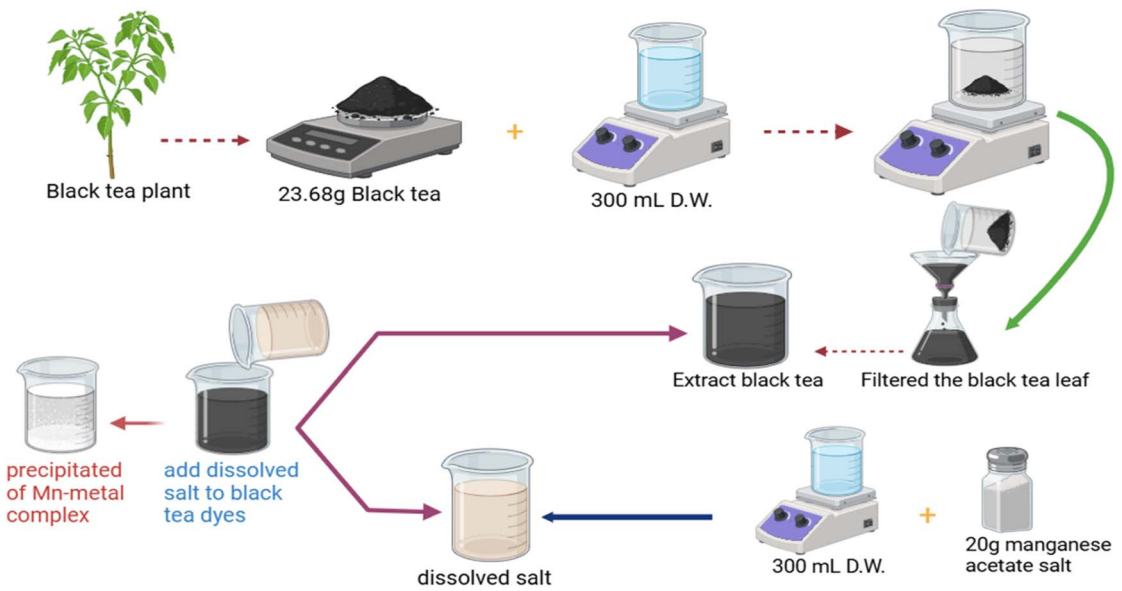

Scheme 1 Schematic representation sample preparation method of polymer complex-based PEO.

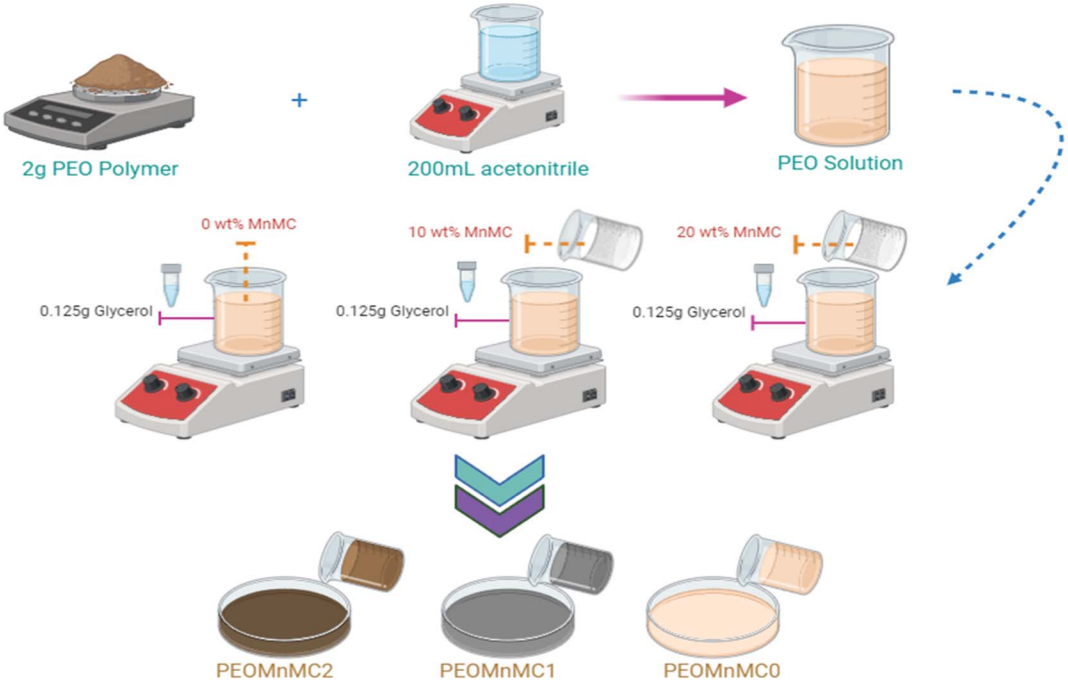

Scheme 2 Synthesis of PEO: Mn–metal complex procedure to produce freestanding solid polymer composite films.

infrared (FTIR) determines the chemical interactions between the metal complex Mn–polyphenol and the PEO polymer. An optical microscope (Am Scope, Fixed Microscope Adapter FMA 050) with a digital camera (14 MP APTINA COLOR CMOS ULTRA-FINE COLORE ENGINE INSIDE) was used to evaluate the composites' morphology. The polymer films were analyzed using a Spotlight spectrophotometer (TENSOR-27) within a wavenumber range of 500 cm^{-1} to 4000 cm^{-1}, with a resolution of 2 cm^{-1}. UV-visible spectra of the composite films PEOMnMC0, PEOMnMC1, and PEOMnMC2, were acquired with the PerkinElmer double-beam UV-vis-NIR spectrometer (Lambda 25) for absorption measurements, also investigating their structural and optical characteristics. Making use of the absorbance and transmittance facilitates investigation of the other fundamental optical properties such as band gap, dielectric constant, refractive index, absorption coefficient, and localized density.

3. Findings and discourse

3.1. X-ray diffraction (XRD) investigation

Both high-order and possible amorphous peaks were identified using the deconvolution method for the XRD spectra.[48] Fig. 1 shows the Mn(II) compound's XRD spectrum. This signifies the amorphous characteristic of the synthesized Mn(II)-complex, emphasizing that no crystalline peaks appear in the 2θ degree zones. A single hump manifests over a range between 2θ = 23.15° and 2θ = 41.25°. The XRD pattern obtained in this investigation is fairly comparable to that documented in earlier studies.[26,49,50]

The XRD spectra of the undoped and doped PEO film are displayed in Fig. 2. For the PEOMnMC0 film, two narrow peaks indicate that the crystalline phase is still predominant within the structure. Two primary features were observed: high-intensity diffraction peaks at (25.09°), and peaks of small intensity at the lower angle (20.89°) and these distinct diffraction peaks allow for the identification of crystalline and partially crystalline structures of PEO polymers.[39,51] This results from the systematic arrangement of polyether side chains and robust hydrogen bonding among PEO chains.[37] Earlier research claimed that the peaks approximately at 22° and 18° are corresponded to the (112) and (120) planes.[52] Fig. 2 illustrates the reduction and shifting of the XRD peak intensities resulting from incorporating the Mn(II)–polyphenol combination. This

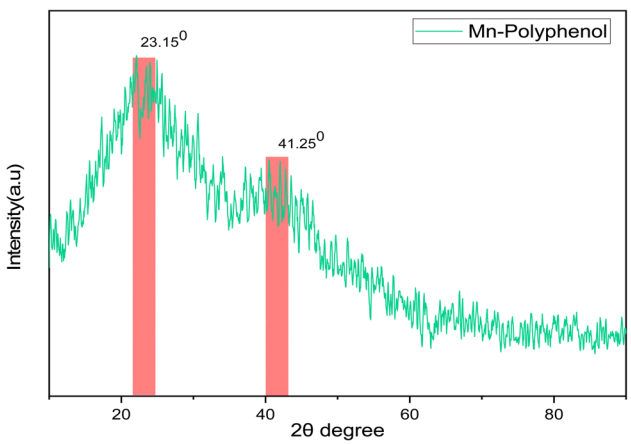

Fig. 1 The XRD pattern displays the Mn–polyphenol complex.

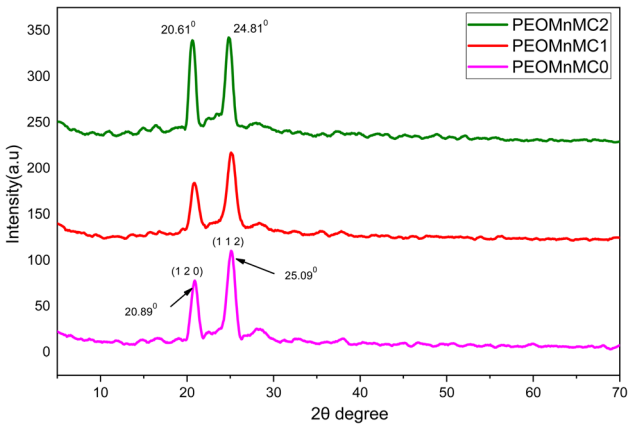

Fig. 2 XRD pattern for pristine and altered PEO films.

indicates that the crystalline structure of the PEO is being distorted by an expanding amorphous region.[53] Morphological studies may give more insights into this behavior. Crystallinity declination is due to the complexation between Mn–polyphenol and PEO.[2,54] The firm peaks that emerged at greater concentrations of Mn–polyphenol (20 mL) indicate the decrease in the amorphous phase and the subsequent rise in crystallinity. Metal complex particle aggregation was formerly thought to cause an increase in polymer crystallinity at high additive concentrations. When the filler particles group together, the host polymer's polar groups are attracted to one another because of the preexisting hydrogen bonding, which increases crystallinity.[53] This will may responsible for unsystematic change in crystalline peak intensities. The PEO: Mn–polyphenol complex was produced based on the results of the XRD investigation.

3.2. Morphological study

Studies have validated the effectiveness of optical microscope (OM) approach to study the morphological appearance of pure PEO and PEO composites.[22,39,53,55] The manufacturing process, temperature, concentration, and dopant material are some of the variables that impact the structural morphology of PEO films.[22] The crystalline areas, which are made up of many platelets or lamellae extending from a nucleating center (so-called spherulites), have been verified by earlier research. The dark areas in between the adjacent lamellae are still amorphous.[56–59] Thus OM approach is crucial to distinguish the crystalline and amorphous regions in semi-crystalline polymers such as PEO. Fig. 3(a–c) displays OM images of pure PEO and PEO films with insertion of Mn–polyphenol complexes. Several large-diameter spherulites were seen in the pure PEO film (Fig. 3(a)). Meanwhile, the spherulite structure completely broke down into tiny spherulites and dark areas were found to increases which an evidence for amorphous phase enhancement when 10 mL of suspended Mn–polyphenol was added to pure PEO, as seen in Fig. 3(b).[53] The random distribution of Mn–polyphenol in the PEO structure and their interaction with functional groups of PEO in the composite film may be one reason for this deformation.[60] As shown in Fig. 3(c), increasing the quantity of Mn–polyphenol to 20 mL results in more spherulites and smaller spherulites than pure film. Therefore, the results of the morphological examination supported the XRD analyses. Phase separation was absent in the hybrid polymer film because the PEO: Mn–polyphenol composite showed crystalline (spherical morphology) and amorphous (dark areas) phases. The presence of metal complexes prevented crystallization; in other words, the PEO chains stopped the crystalline lamellae from extending in a certain direction, decreasing crystallinity.[53] The results of the current study establish that green synthesized metal complexes which enriched with many functional groups such as NH, OH, C=O and C–O–C are essential to disrupt the hydrogen bonding among the PEO chains and thus the crystalline phases of PEO will be scarified.

3.3. Fourier transform infrared (FTIR) analysis

The investigation relies on the molecular absorption spectroscopic method that provides useful molecular-level information on polymer composites while adhering to Beer–Lambert Law. When infrared (IR) radiation is absorbed, molecules are excited from lower to higher vibrational energy levels. The IR signals that result from these vibrational transitions will be useful for diagnosing organic functional groups and for a variety of spectroscopic investigations.[61] The extracted black tea dye's FTIR spectrum is shown in Fig. 4(a). The intense broad region at 3410 cm^{-1} is attributed to the N–H and O–H stretching modes.[61] Whereas previous study indicated that the wide range between 3500 cm^{-1} and 3000 cm^{-1} was associated with N–H stretching in amines I and II, as well as amides and O–H stretching of hydroxyl groups (phenols, alcohols, and carboxylic acids).[62] A robust apex that was centered about 2930 cm^{-1} is linked to the CH stretching mode in carboxylic acid and aliphatic groups (R–COOH).[62–64] The C=O stretch in polyphenols, the C=O vibration of bonded conjugated aldehydes, ketones, quinines, and esters, and C=C stretch in aromatic rings can be connected by the robust band 1635 cm^{-1}.[65,66] Furthermore, a band at 1045 cm^{-1} has been identified as the outcome of amino acid C–O stretching.[65] According to earlier studies, black tea extracts display multiple bands.[65,67–69] The bending of the C–OH bonds and the stretching of the –OH and C–O groups are responsible for broad bands at about 3282 cm^{-1}, 1142 cm^{-1}, and 1032 cm^{-1}, respectively. Based on published study, the bands at 2922 cm^{-1} and 2848 cm^{-1} are ascribed to symmetrical and asymmetrical C–H stretching.[67] The wake band was reported to be caused by C–H out-of-plane bending, ranging from 819 cm^{-1} to 831 cm^{-1}.[67] The FTIR spectrum distinctly indicates that primary functional groups in tea comprise amino acids, phenols, and carboxylic acids. In order to synthesize metal-complexes from transition metal salts, the researchers found that the dye made from black tea is rich in ligands. Based on previous studies, polyphenol and metal positive ions are capable of mixing to create metal–polyphenol coordination, as seen in the colloidal suspension and the green mixture at the container's bottom and top, respectively.[29,64,70,71] A prior investigation demonstrates the feasibility of effective attribution (Ce^{+3}–polyphenol, Cd^{+2}–

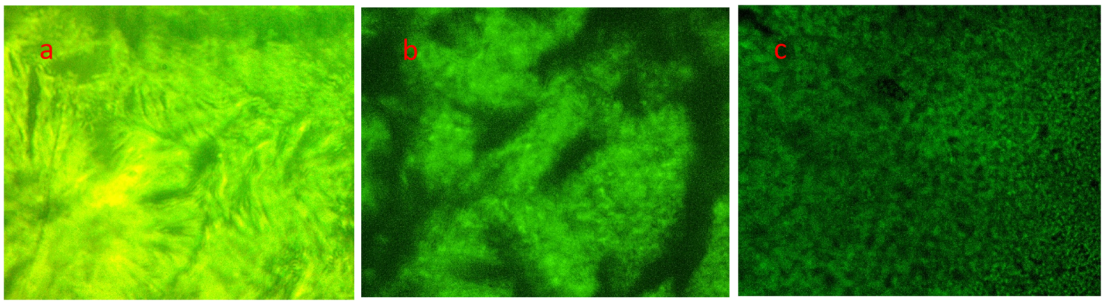

Fig. 3 (a–c) OM images for (a) PEOMnMC0, (b) PEOMnMC1, (c) PEOMnMC2 films.

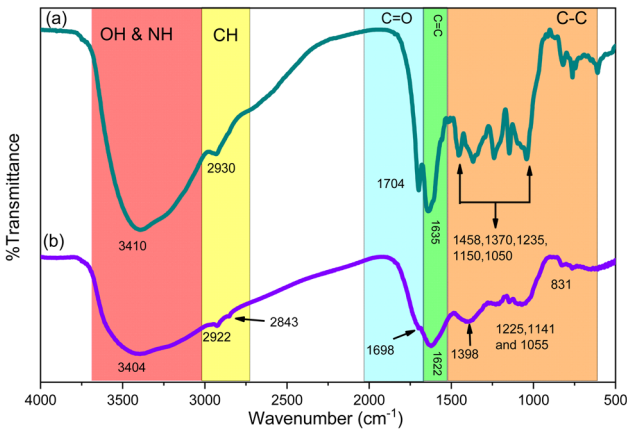

Fig. 4 FTIR spectra of, (a) extracted black tea and, (b) Mn–polyphenol.

polyphenol, Co^{+2}–polyphenol, Al^{+3}–polyphenol) complexes.[13,26,72,73] Also, Brza *et al.*[74] Ce^{+3}, Cu^{+2}-, and Cd^{+2}-complexes were prepared utilizing the green technique with a solution of black tea leaf extract. The FTIR spectrum corresponding to the Mn–polyphenol combination is illustrated in Fig. 4(b). As was previously indicated, polyphenols interact with Mn(II) ions to produce Mn(II)–polyphenol complex solutions. Although they displayed shifting and diminishing intensities, The peaks seen in the FTIR spectrum of black tea are also recognized in the FTIR spectra of Mn(II)–polyphenol compounds. It's intriguing to note that when the Mn(II)–polyphenol compounds formed in black tea, the bands seen at 2930 cm^{-1} changed and almost disappeared, showing up at 2922 and 2843 cm^{-1}, respectively. Comparison of Fig. 4(a) and (b) clearly indicates that peak values in the 1700–400 cm^{-1} range nearly shift. This phenomenon can be elucidated by the formation of bonds between Mn ions and polyphenols, which results in vibrational attenuation and an increase in the diminishing mass.[17,29] The development of metal complexes with polyphenols arises from the interaction between ligand pairs and vacant orbitals in Mn ions.[72] The interaction between Mn ions and caffeine and polyphenols in tea extracts can be evaluated using FTIR analysis, with three potential complexes illustrated in Fig. 5. Also, Scheme 3 shows Ligand Field Theory to propose the Mn metal complex formation of $[Mn\ (OH)_6]^{4-}$ and $[Mn\ (NH)_6]^{2+}$.

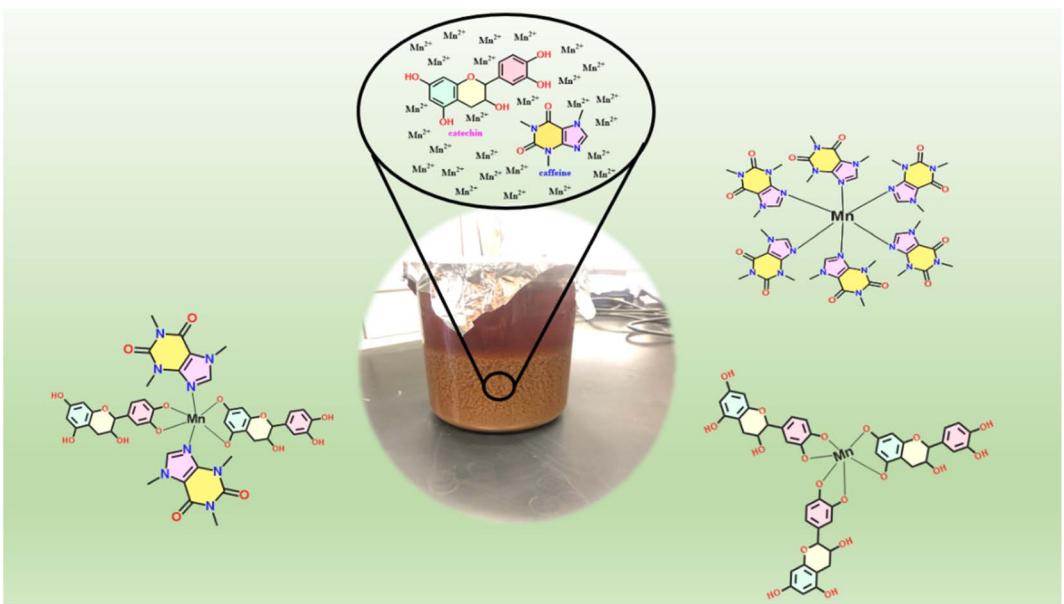

Fig. 5 The Mn–polyphenol molecule can arise in three different ways.

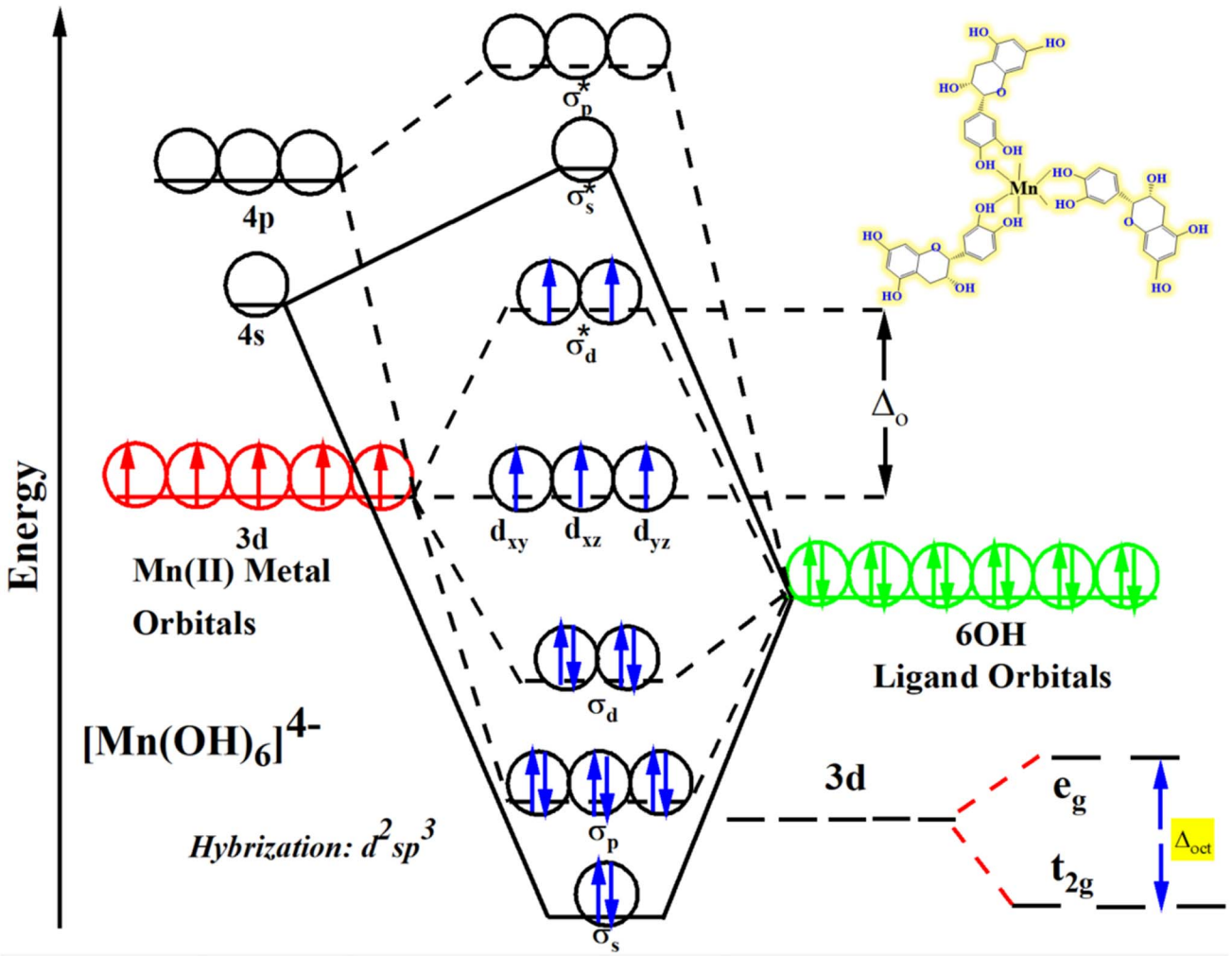

Scheme 3 Proposed pair electron sharing between Mn metal and ligand orbitals.

FTIR spectroscopy may identify the creation of complexes between PEO and Mn–polyphenol. Fig. 6 shows an illustration of the samples' FTIR spectra. The following vibrational modes were associated with the peaks in the PEOMnMC0 FTIR spectral: the broad peak at around 3338 cm^{-1} was linked to –OH stretching.[75] The peak appeared at 2877 cm^{-1}, which corresponds to the $-CH_2-$ symmetric stretching vibration.[76,77] CH asymmetrical stretching frequency of 1965 cm^{-1} in pure PEO.[78] The 1456 cm^{-1} peak was associated with asymmetric bending, and the peak about 11 093 cm^{-1} was associated with C–O–C stretching; the peak at 840 cm^{-1} was associated with CH_2 rocking.[53,79] The FTIR results acquired in this investigation closely mirror those reported in prior studies.[22] The peak at 3338 cm^{-1}, corresponding to the hydroxyl group –OH, almost vanished with the increasing concentration of Mn–polyphenol, indicating a reduction of the hydroxyl group and verifying the interaction between the PEO polymer and Mn–polyphenol.[77] In addition, several peaks were shifted in location and were generally less intense. The peaks at 1456 and 1039 cm^{-1} in the PEOMnMC0 sample moved to 1448 and 1085 cm^{-1}, respectively. Pristine PEO often transitions to a lower frequency region when Mn–polyphenol concentrations increase. Complexation transpires due to the elongation of bond length due to reduced wavenumber.[10,78] The locations and intensities of the peaks exhibited minor changes as the content of Mn–polyphenol in the samples increased. The increase in molecular weight (MW) due to adsorption has reduced the vibrational intensity associated with a functional group.[17]

3.4. Absorption study

The optical transition characterizes the electron transition from ground state to higher energy states.[1,80] UV-visible absorption spectroscopy was employed to characterize the Mn–polyphenol complex and extract black tea, as shown in the Fig. 7(a and b). The absorption has been investigated over spectral range from UV to visible. Different kinds of electronic transitions could occur within the structure. Because it sheds light on the energy gap (E_g) in both crystalline and non-crystalline materials, UV-visible spectroscopy is a useful investigative technique. According to molecular orbital theory, electrons in the σ, π, and n-orbitals are promoted from lower energy levels to greater energy states when polymeric materials absorb frequencies of

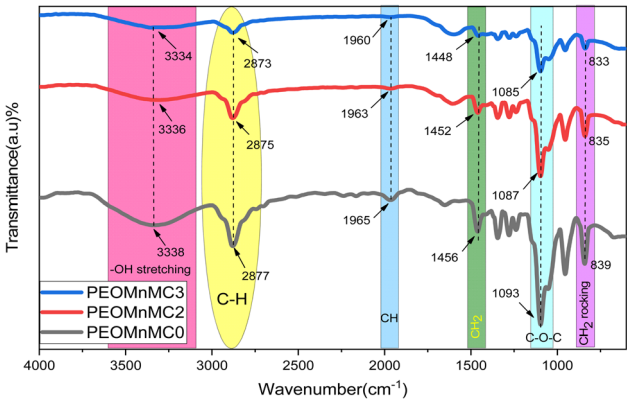

Fig. 6 FTIR spectra of undoped and modified PEO polymer.

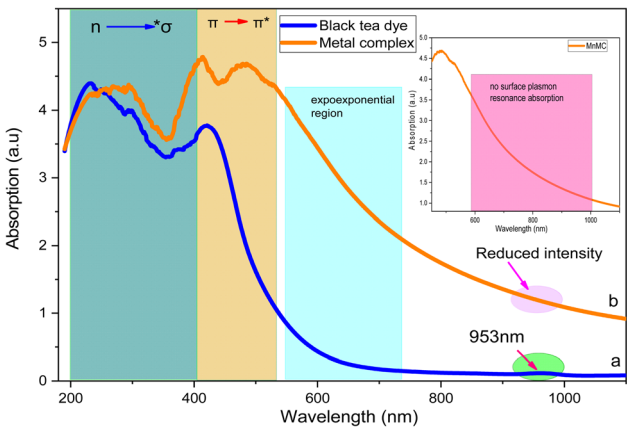

Fig. 7 (a and b) Optical absorption spectra of extracted black tea and Mn(II)–polyphenol.

light in the visible and ultraviolet spectrums.[81] The presence of several organic constituents, such as polyphenols, alkaloids, glucides, amino acids, volatile compounds, proteins, minerals, and trace elements, makes the tea samples shown in Fig. 7(a) chemically complex.[82] Within the visible spectral range (400–800 nm), the spectra exhibited an absorption peak at 420 nm, indicating that the majority of light absorbed by tea leaves lies within the visible region.[83] It can be concluded that the natural dyes made from black tea enriched with ligands are useful and eco-friendly dyes that are employed to form coordination compounds and thus produce metal complexes, as demonstrated in Fig. 5.[26] While movements like $\pi \rightarrow \pi^*$ and $n \rightarrow \pi^*$ of (catechins) CTH, methylxanthines, and caffeine require far lower frequency and consequently take place at larger wavelengths, the electronic transition of $n \rightarrow \sigma^*$ is caused by the UV (190–420 nm) electronic transitions.[22,41,80,84] The study's UV-vis spectrum result is comparable to Wang *et al.*[85] report on iron–metal complexes. A prior study also found that the absorbance band emerged between 200 nm and 350 nm, which corresponds to the electronic transition of n–π* of methylxanthines, which are made up of caffeine, theobromine, and theophylline. Caffeine's C=O chromophore band absorbance is visible at about 275 nm.[26,86–88] In the UV-visible spectrum, metal nanoparticles ought to exhibit surface plasmon resonance absorption.[89] There is no observable surface plasmon resonance absorption of Mn–polyphenol in this spectrum. This suggested that the Mn–polyphenol complex's metal-like properties on the particle surfaces could not be attributed to the capping of polyphenols.[85,90] An SPR apex in the 500–800 nm range has been observed for copper nanoparticles in chitosan-based polymer electrolytes, confirming a prior study.[91] Also, Aziz *et al.*[92] emphasize that the CS: AgNt system's production of silver nanoparticles is connected to the wide apex at 422 nm. The π electrons exist in both pure PEO and modified samples due to absorption peaks seen at higher wavelengths, particularly in the 550–750 nm region (exponential curves).[93] In a recent study on green tea dye, the peak was found at 671 nm. Conversely, the metal complex's absorption spectrum shows the same peak but with less intensity. In the current study, black tea dye also showed the same peak in the 953 nm range, even though the Mn(II)–polyphenol complex produced an Albert peak with less intensity. This finding implies that Mn acetate and black tea have a beneficial interaction (see Fig. 7(a and b)). Also, both (black tea dye and metal complex) exhibit exponential curves in the visible region.[94] Because of the interaction between the inorganic metal and the organic ligand, the metal–organic compound has special optical and electrical properties with great potential for use in optical electronic devices.[95] Moreover, researchers can use UV-visible analysis to study the interaction between the coordination compound and PEO polymers. In order to observe the variations in absorption spectrum, locations brought about by the chemical reaction between the complex of metals with PEO, various amounts of the Mn–metal complex were incorporated into PEO. When the metal complex was incorporated into the PEO polymer, the absorption moved from the ultraviolet to the visible spectrum, indicating a shift from high energy to low energy. This investigated the positive interaction between the PEO polymer and Mn(II)–polyphenol.

4. Optical properties

4.1. Absorption and transmission

Because polymers are widely used in electronics and optical technologies like chromic displays and electronic parts like light-emitting diodes (LEDs), polymer lasers, and organic photovoltaic devices, their optical characteristics have been thoroughly researched.[64] Fig. 8(a) at lower frequency, it appears like the films are almost transparent in PEO only. Additionally, displays the absorption spectra of metal complex-doped PEO. Various electronic transitions can occur in polymers. The $\pi \rightarrow \pi^*$ electronic transition type, which originates from unsaturated bonds, primarily C=O and C=C, found in the polymer's tail head, is responsible for the absorption band that spans between 200 and 300 nm. The addition of Mn–polyphenol clearly caused the absorption spectra to shift to longer wavelengths.[34,39] Furthermore, absorption bands were absent in all visible zones for undoped PEO, indicating that it is an insulator. In contrast, the visible region of PEO: metal complex composite films showed broad absorption bands. Particularly, when the

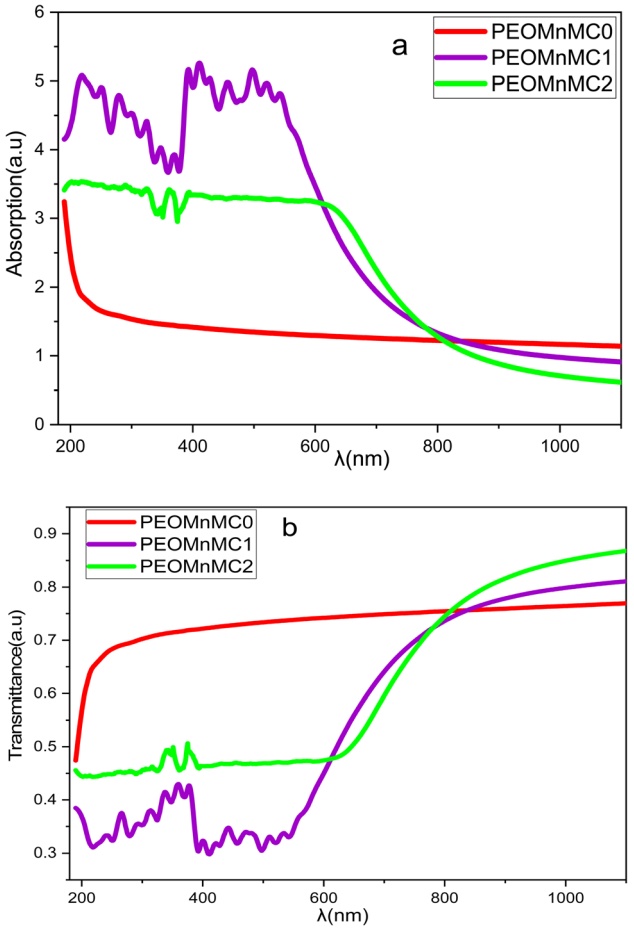

Fig. 8 (a and b) (a) Absorption spectra, (b) transmission spectrum of doped with and unmodified by PEO.

concentration of the suspended metal complex was raised to 20 mL, the absorption peak became more intense.[53] It is evident that all of the samples' spectra of absorption drop as wavelength increases while increasing when metal complex levels rise.[96] The doped samples' absorption spectra exhibit a shift towards longer wavelengths, indicating that these materials may have narrow band gaps.[97] Fig. 8(b) shows the transmission spectra for the unaltered and modified PEO films. As the concentration of Mn–polyphenol rises, there is a shift towards lower UV wavelengths, resulting in a decrease in the transmittance of the polymer films.[98] In optoelectronic applications, conjugated systems with both single and dual bonds have been regarded as a significant class of materials because of their strong pi-bonding orbital value. These significant shifts show that π-delocalization takes place throughout the polymer chain. π-Conjugated polymers are usually low-bandgap, semiconducting polymers.[99] The band edge is the location where transmission begins to drop.

4.2. Absorption edge

The absorption edge, in particular, has proven crucial in identifying the electrical structure of materials by optical absorption research. The optical spectrum of absorption can reveal direct as well as indirect transitions inside the band gap.[100] Moreover, the optical absorption coefficient of a material indicates how well it can absorb photons.[101] The light absorption spectra are crucial in measuring the energy gap of crystalline and non-crystalline materials. The fundamental absorption, which is equivalent to the electron moving from the stable state to the energetic state, may be used to ascertain the kind and worth of the (E_g).[102] The absorption edge is the region where electrons shift from a low-energy to a higher-energy level as a result of light absorption.[103] From the absorbance (A), which can be determined from UV-visible spectroscopy, the absorption coefficient as a function of frequency or the relative rate at which light intensity decreases may be computed, $\alpha(\nu)$. a set of data using Beer–Lambert's formula.

$$\alpha = \left(\frac{2.303A}{d}\right) \quad (1)$$

where (d) represents the sample's width.[99,104] Fig. 9 displays the α *vs.* photon energy E_{Photon} of many pristine and altered PEO films made with Mn–polyphenol. By extrapolating the linear segment of the α *versus* E_{Photon} curve to zero absorption, we estimated the absorption edge values shown in Table 1. This was a simple method of computing the absorption coefficient. In the present computation, the addition of 20 wt% of Mn–polyphenol complexes reduced the absorption edge of a pure PEO to decrease from 5.3 eV to 1.42 eV. When the dopant concentration is raised, the reduction of the absorption edge might be interpreted as an enhancement of interchain interactions among the polymer composite chains. Consequently, the density of conjugation stacking increased. In other words, modifying the absorption edge may facilitate the creation of novel effective traps within the optical bandwidth. Consequently, electrons in the present state transitioned from the apex of the valence band to the nadir of the conduction band.[105,106] The dispersion and complexation of Mn–polyphenol inside the PEO matrix account for broadening the absorption edge.[100] Accordingly, it is assumed that the band gaps determined using various methods are near the absorption edge values.[53]

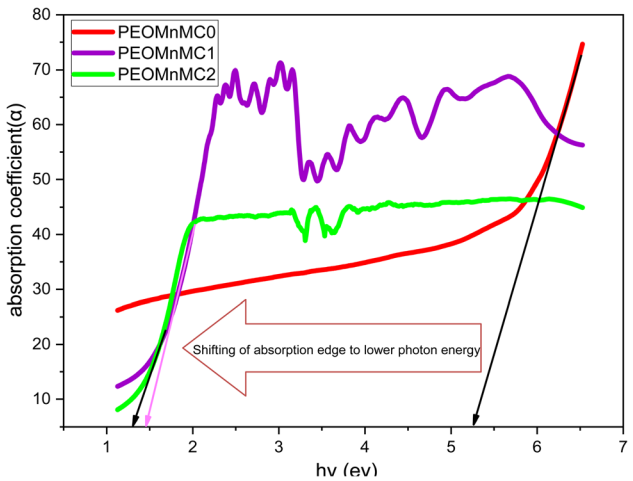

Fig. 9 E_{Photon} *versus* $\alpha(\nu)$ for undoped and composite samples.

Table 1 PEO samples, both undoped and doped, have different values for the absorption edge and Urbach energy

Sample composition	Absorption edge (eV)	Urbach energy (eV)
PEOMnMC0	5.3	1.3405
PEOMnMC1	1.45	1.4136
PEOMnMC2	1.42	1.6126

4.3. Refractive index (*n*)

The refractive index is a fingerprint of a polymeric substance. A polymer is termed an isotropic polymeric substance when light propagates through it at a uniform velocity in all directions. When light travels through a polymer at varying velocities in a single direction, the polymer is classified as an anisotropic polymeric material.[4] Therefore, refractive index (n) is considered as an essential optical parameter associated with microscopic atomic interactions. Particularly in designing and manufacturing optoelectronic devices. Mathematically, It can be computed using the extinction coefficient (k) and reflectance (R).[6,107]

$$n(\lambda) = \sqrt{\frac{4R}{(1-R)^2} - k^2} + \frac{1+R}{1-R} \quad (2)$$

Using the formula $k = \alpha\lambda/4\pi d$, where (α) is the samples' absorption coefficient and (λ) is their wavelength and (d) is their thickness, the extinction coefficient (k), or the imaginary component of the complex index of refraction was calculated for each sample.[34] The following formula can be used to alter the index of refraction of a substance if it absorbs the light that hits it.

$$\tilde{n} = n + ik \quad (3)$$

where k is related to the absorbed energy, $\tilde{n}$ is the complex index of refraction, and n is the actual refractive index.[108] It is also evident from another numerical statement for the imaginary part of the complex refractive index that the reflectance (R) may be calculated from the transmission (T) and absorption (A) values ($R = 1 - (A + T)$). Beer's law is used to calculate the T values ($T = 10^{-A}$).[72] Applications in the areas of materials science, optical technology, and optical photonics depend on a better understanding of how undoped and modified polymer substances interact with light. This helps to clarify features like light transmission and reflection within the material. Nevertheless, in order to comprehend how the insertion of the metal complex alters light propagation within the material when a polymer is doped with it, the optical study is required.[93] The refractive index is the ratio of the speed of light in a vacuum (c) to the speed within a material.[109] As shown in Fig. 10, the index of refraction tends to remain constant at lower energies and falls as the wavelength of the incident photon increases. Generally speaking, both density and polarizability affect the index of refraction. Therefore, adding more charge carriers to the host polymer is means that a metal complex is added to PEO films. According to the Lorentz–Lorenz formula, this will lead to a higher index of refraction because there will be more polarizable molecules and higher densities.[98,106,110]

It is well understood that the transparency of various optical materials is determined by its refractive index. When materials are completely transparent, $n(\lambda)$ is near to one.[22] In this study, when we add the metal complex to a pure polymer, two factors contribute to the decrease in n; firstly, the PEO polymer in its pure state lacks transparency and is opaque. However, the composite polymer gets closer to transparency as the concentration of the metal compound rises. Secondly, the PEO polymer in its pure state exhibits a high ordering structure, also known as high crystallinity. The –O group present in PEO facilitates a high level of crystallinity.[111] It's fascinating to note that high-order atoms have demonstrated a comparatively elevated index of refraction that is unaffected by wavelength or surface strikes of light.[64]

4.4. Wemple and DiDomenico (W–D) model

In the optoelectronics field, the optical dispersion characteristics are the most important parameters to comprehending the degree of disorder. These parameters can be thoroughly calculated using the (WDD) single-oscillator model, which is expressed as:

$$\left(n^2 - 1\right)^{-1} = -\frac{1}{E_0 E_d}(h\nu)^2 + \frac{E_0}{E_d} \quad (4)$$

At ($h\nu \approx 0$) it becomes:

$$n_0 = \sqrt{1 + \frac{E_d}{E_0}} \quad (5)$$

where $n \approx n_0$ at longer wavelength (n_0 is a static refractive index), E_d is the dispersion energy, and E_0 is the average excitation energy of electronic transitions (oscillator energy).[107,112] The average strength of the oscillator or inter-band optical

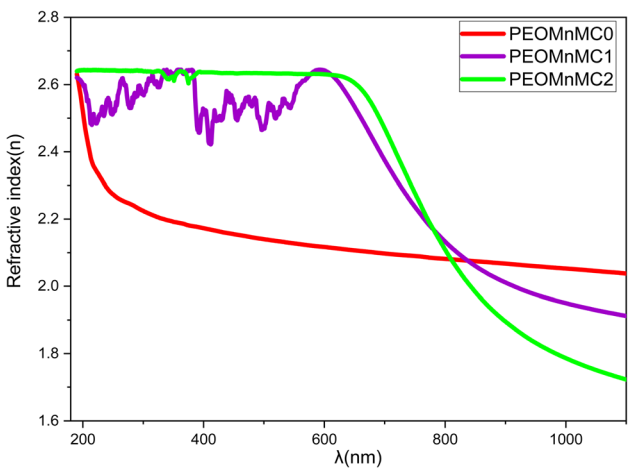

Fig. 10 Refractive index *vs.* function wavelength.

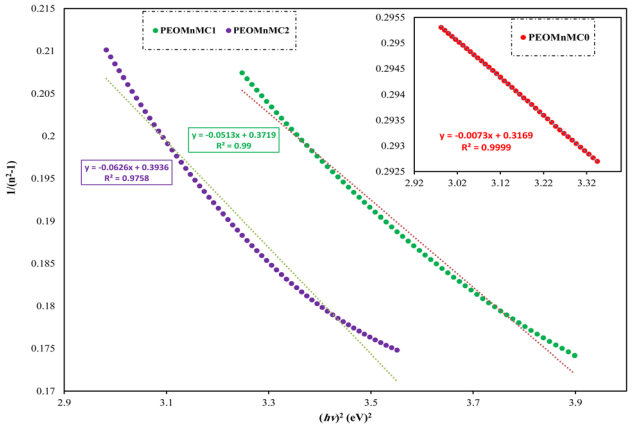

Fig. 11 Variant $(n^2 - 1)^{-1}$ against $E_{Photon}{}^2$ for undoped and modified PEO.

transition is represented by the dispersion energy, which is associated with the chemistry of the material. The oscillator energy is linked to the energy gap's scale.[113] Then E_0 and E_d were determined from $(n^2 - 1)^{-1}$ *vs.* $(h\nu)^2$in Fig. 11, E_0 and E_d values can be calculated from $1/E_dE_0$ (slope) and E_0/E_d (intercept) on vertical axis as depicted in Fig. 11. The static refractive index n_0 values for pristine PEO and altered PEO films are given in Table 2 and may be computed using eqn (5).[114,115]

4.5. Dielectric constant study (ε^*)

It is well known that variations in the optical dielectric constant produce the essential electromagnetic transition in polymer composites. One can quantify a bulk material's energy loss capacity by measuring the quantity of electrons on its surface. Conventionally, the dielectric constant is taken as its two main parts: imaginary (ε_i) and real (ε_r). The real part determines a given material's capability to reduce electromagnetic wave speed. On the other hand, the imaginary part enables us to calculate the efficiency of absorbing energy due to polarization is computed. Both n and k values are related to the real and imaginary components ε^*.[17]

$$\varepsilon^* = \varepsilon_r + i\varepsilon_i \quad (6)$$

The Spiter–Fan equation is validated by Fig. 12, which shows the linearity of the graphs showing the direct link between the ε_r and λ^2 within particular ranges.

$$\varepsilon_r = n^2 - k^2 = \varepsilon_\infty - \frac{e^2}{4\pi^2 c^2 \varepsilon_0} \times \frac{N}{m^*}\lambda^2 \quad (7)$$

ε_∞ denotes the material's dielectric response at high frequencies within the lattice, especially at short wavelengths. In this context, we establish the following constants: the electron effective mass (m^*), the dielectric constant of the free space region (ε_0), the speed of light (c), the charge of an electron (e), and the concentration of charge carriers (N). The ratio of the electron's effective mass to the free concentration of carriers is denoted by N/m^* and ε_∞. Both parameters were acquired by looking at the slopes and intercepts of Fig. 12, which is

Table 2 Dispersion and oscillator energy calculate from theoretical Wemple–DiDomenico (WD) and static refractive index

Concentration	E_d	E_0	n_0
PEOMnMC0	20.7911	6.5887	2.039
PEOMnMC1	7.2398	2.6925	1.9206
PEOMnMC2	6.3707	2.5075	1.8817

displayed in Table 3.[94,116,117] When the Mn–polyphenol compound is added to (PEO), the localized density between the polymer's valence and conduction band increases as the metal complex's amount increases. The polymer composite's energy bandgap decreases as a result of this rise in localized state density.

4.6. Inter-band transition strength (J_{CV})

The complex dielectric constant ε^* is also linked to J_{cv}, the latter is proportional to the likelihood that an electron would transition from the lowest energy state to the highest energy state with transition energy.

$$J_{cv} = \mathrm{RE}\, J_{cv} + \mathrm{IM}\, J_{cv} = \frac{4\pi m_0{}^2}{e^2h^2}\frac{E^2}{2}(\varepsilon_1 + i\varepsilon_2) \quad (8)$$

The real and imaginary parts of the interband transition strength are denoted by RE J_{cv}, IM J_{cv}, the electron's mass (m_0), the photon energy (E_{photon}), the electron's charge (e), and the plank constant (h). J_{cv} has units of g cm^{-3} and is proportional to the transition probability. For computational convenience, we take the factor $\left(\frac{4\pi m_0{}^2}{e^2h^2}\right)$ in eqn (8), whose value in 8.289 × 10^{-6} g eV^{-2} as unity. Eqn (8) is where the J_{cv} was computed from. Fig. 13(a and b) shows the real and imaginary components of the inter-band transition intensity J_{CV} against photon energy. It increases with photon energy, suggesting that the likelihood of electronic transitions happening increases with photon energy.[118,119]

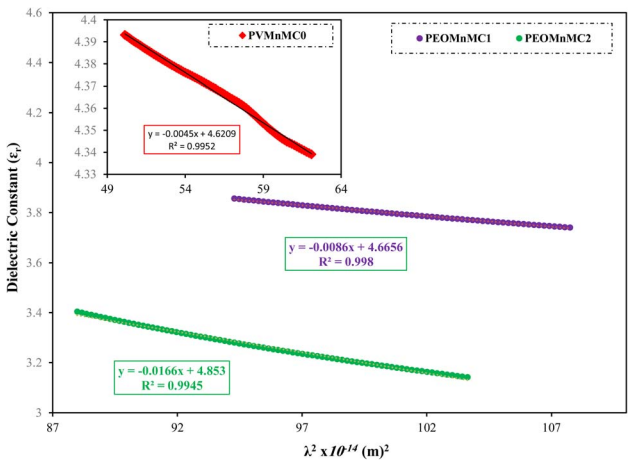

Fig. 12 Illustration of undoped and doped PEO's real part dielectric constant against λ^2.

Table 3 Localized density and dielectric values at lower wavelengths for pristine and composite PEO films

Sample	Localize density $\left(\frac{N}{m^*}\right) \times 10^{55}$	ε_∞
PEOMnMC0	54.7445	4.6209
PEOMnMC1	104.6228	4.6656
PEOMnMC2	201.9465	4.853

4.7. Optical bandgap study

4.7.1 Tauc's model and optical dielectric loss. Depending on the material's band structure, the fundamental absorption process is frequently defined as the flow of electrons between the valence and conduction bands, controlled by certain selection principles and marked by a noticeable rise in the absorption zone. Different transitions are known, where materials with direct band structures exhibit momentum conservation throughout the transition, whereas amorphous semiconductors with indirect band structures do not exhibit electronic momentum conservation.[120] Two techniques were used in this paper's band-gap analysis, which were based on both theoretical and experimental approaches. The theory of optical absorption served as the foundation for Tauc's technique. It is a popular method for studying the band gap, which links the absorption coefficient and photon energy. However, in order to study the band gap, theoretical physicists have created a number of models based on quantum techniques. According to theory, all inherent effects associated with processes of light–matter interaction are contained in the optical dielectric function.[91] Using Tauc's equation, the connection between the incoming photon energy and the absorption coefficient for non-crystalline materials may be found as follows:.[121,122]

$$\alpha hv = \beta(hv - E_g)^L \quad (9)$$

where the optical energy bandgap is denoted by E_g and a constant by β. Depending on the type of electron transitions that are susceptible to optical absorption, n is an exponent constant. The direct allowed, indirect allowed, forbidden direct, and forbidden indirect electron excitations are represented by the exponent L values of 1/2, 2, 3/2, and 3, respectively.[121] Fig. 14 depicts the types of transitions related to electrons based on Tauc's model. Fig. 15(a–d) shows the graph of $(\alpha hv)^{1/L}$ against of E_{Photon} for all composite samples. The intersection of the extrapolation of the linear portion of the plots to the energy axis yielded the direct bandgap values. All of the samples' bandgap values were calculated and are shown in Table 4. The doped samples were found to have a lower optical bandgap (E_g). In accordance with previous studies, organic polymers, functional materials, and composites with suitable optical bandgaps are crucial for photonics, organic light-emitting diodes (OLEDs), and optoelectronic device applications.[121] Large band gap materials are typically insulators, while semiconductors are materials with smaller band gaps. Therefore, due to its large bandgap at about 5.5 eV, pure PEO is an insulator. This suggests that there is no free carrier absorption and that inter-band transitions only become important at rather high photon energy (above visible).[40]

It has been shown that the band boundaries in amorphous materials are influenced by various ligand and metallic complex

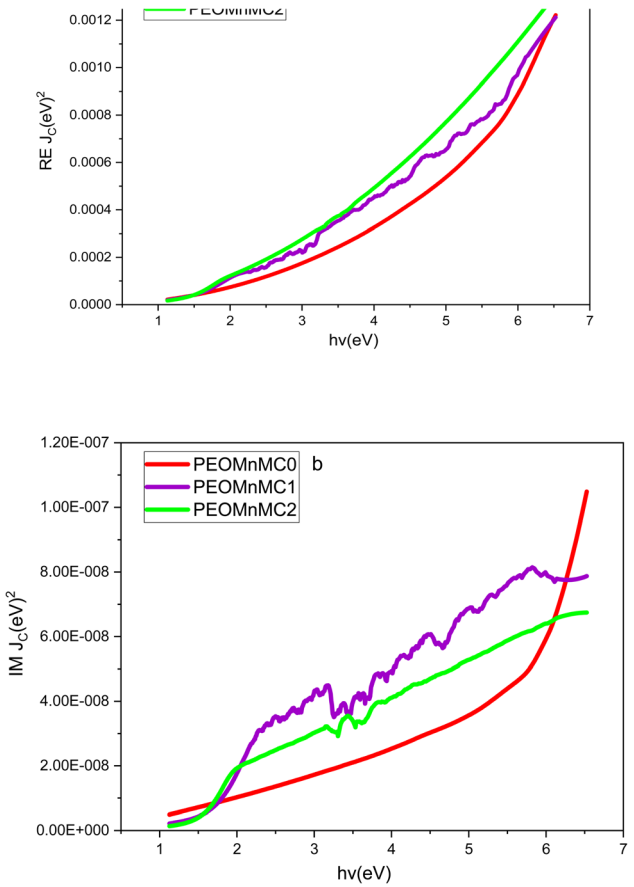

Fig. 13 (a and b) Plot (a) RE J_{CV} and (b) IM J_{CV} against of E_{Photon} of for undoped and alter PEO polymer composites.

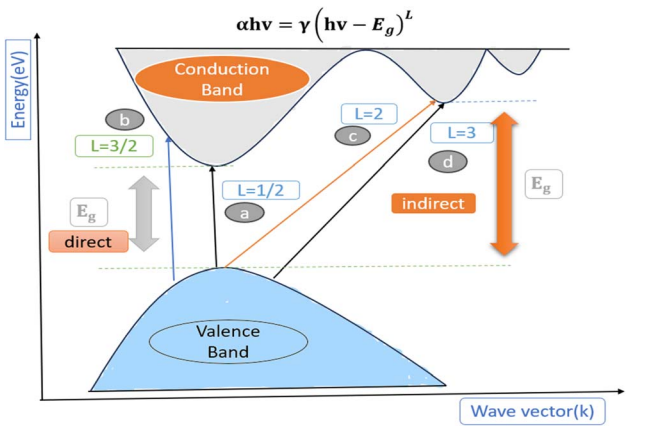

Fig. 14 Typical representation of various types of electronic transition within materials: (a) direct allowed transition, (b) direct forbidden transition, (c) indirect allowed transition, and (d) indirect forbidden transition.

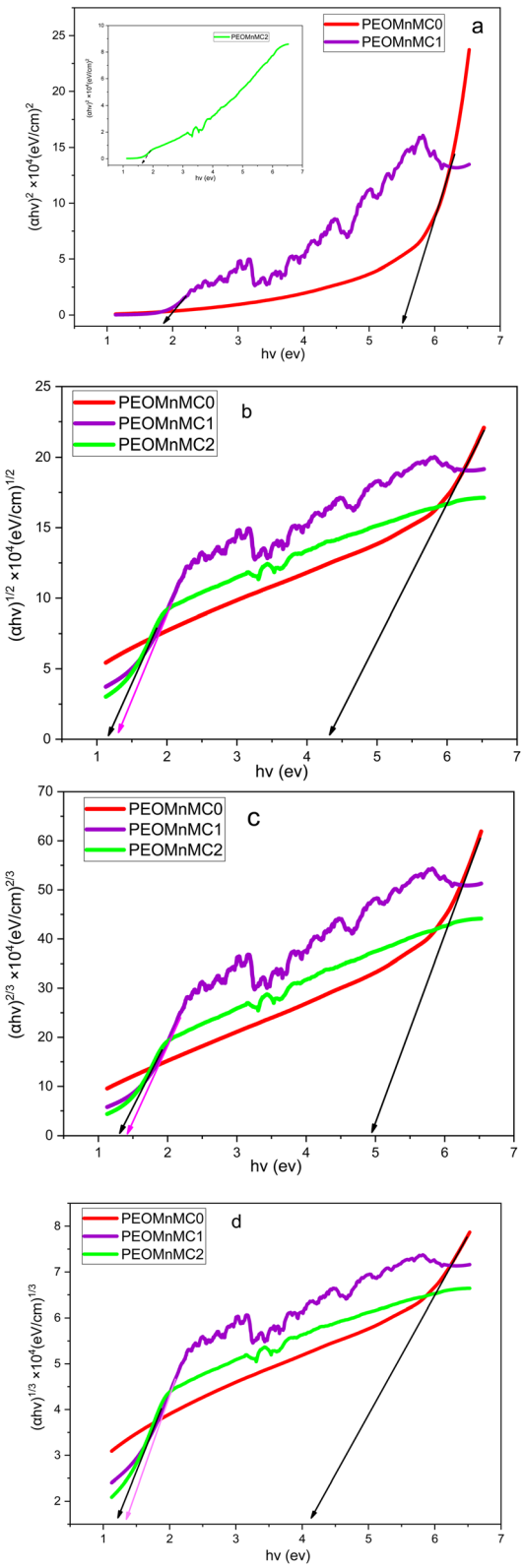

Fig. 15 (a–d) The plot of $(\alpha h\nu)^{1/L}$ against the E_{Photon} of the undoped and modified PEO films.

orbital types. It is challenging to forecast whether the band will be direct or indirect. It should be noted that Tauc's equation by itself is inadequate in this situation to characterize the kind of transition, as four figures must be created based on the values that the exponent takes. Quantum mechanical characterization of the photon–electron interaction in the system is based on time-dependent perturbations of the ground electronic state. Several theoretical investigations have focused on the strong association between optical dielectric loss (ε_i) and the band structure of the materials. The imaginary component ε_i of the dielectric function can be expressed as follows:[40,123]

$$\varepsilon_i = \frac{2\pi e^2}{\Omega\varepsilon_0}\sum_{K,V,C}|\Psi_K^C|u,r|\Psi_K^V|^2\delta\left(E_K^C - E_K^V - E\right) \quad (10)$$

The above equation represents the position vector and a vector representing the incident electromagnetic wave polarization as $\rightarrow r$ and $\rightarrow u$, respectively; the incident light frequency and the crystal volume are represented by ω and Ω; the electron charge and permittivity of free space are represented by e and ε_0, while the conduction and valence band wave functions at K are respectively denoted by $\Psi_K^V$and Ψ_K^C. The theoretical models determine that the optical dielectric constant is characterized by a complex function of frequency.[123] Also, it is well known that the optical band gap can be deduced from the fundamental absorption edge in optical dielectric loss spectra.[124] From an experimental standpoint, the obtained refractive index, extinction coefficient, and applied relations below can be used to determine the imaginary portion of the optical dielectric function (ε_i).[34,105,125]

$$\varepsilon_i = 2nk \quad (11)$$

Previous studies have shown that electron transitions from the valence band of energy to the conduction band of energy are directly correlated with the principal peak of optical dielectric loss (ε_i).[120,125–127] Thus, the energy gap can be successfully studied using the ε_i *versus* photon energy. Thus, as shown in Fig. 16, the linear parts of optical dielectric loss spectra may be intercepted with the photon energy axis to get the actual energy gap (E_g). Table 4 lists the estimated values derived from the plot drop in bandgap from 5.5 to 1.4 eV. The kind of electronic transition and the optical band gap can be determined by comparing plots obtained from Tauc's equation with those of optical dielectric loss.[125,128] Quantitatively, Table 4 illustrates the decline in E_g magnitudes with the addition of Mn–polyphenol to PEO polymer. By contrasting the energies from the optical dielectric loss (Fig. 16) with the E_g values in Tauc's model (Fig. 15(a–d)), the types of transitions may be determined. For PEOMnMC0, this means that it is directly allowed ($L = 1/2$), whereas PEOMnMC1 and PEOMnMC2 are both direct forbidden ($L = 3/2$). Because of its nearly crystalline structure, as shown by the XRD analysis results and the Urbach energy discuss in the next section, as well as the coincidence of the valence band's and conduction band's tops in ordered materials, undoped PEO is associated with a direct allowed transition, which is consistent with the theoretical background. This demonstrates how much more practical direct transition is in the case of undoped PEO.[53] This work focuses on the development of polymer composites with narrow optical band gaps that

Table 4 The value E_g from Tauc's model and dielectric loss *versus* E_{Photon}

Sample code	E_g for $(\alpha h\nu)^2$	E_g for $(\alpha h\alpha)^{2/3}$	E_g for $(\alpha h\alpha)^{1/2}$	E_g for $(\alpha h\alpha)^{1/3}$	E_g from ε_i
PEOMnMC0	5.5	4.95	4.5	4.1	5.5
PEOMnMC1	1.9	1.4	1.3	1.35	1.5
PEOMnMC2	1.6	1.3	1.15	1.2	1.4

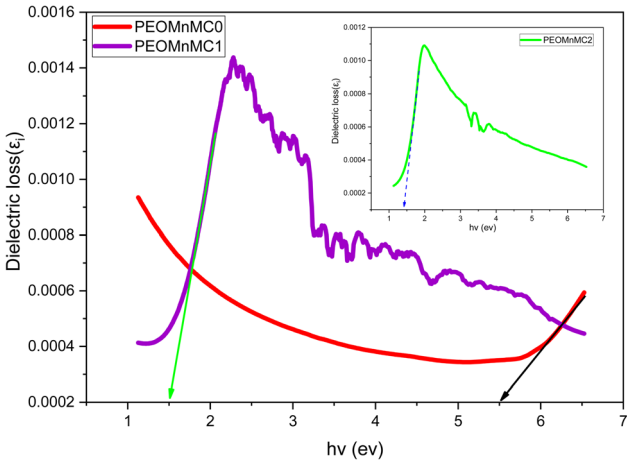

Fig. 16 ε_i *vs.* E_{Photon} for pure and modified PEO.

resemble semiconductor or conductive polymer materials. The bandgap is reduced as a result. It was previously suggested that the decrease in the optical energy band gap could be due to the different localized trap states through the prohibited band gap. The polymer and the loaded metal compound created these localized levels.[39,129] Additionally, the reduction in the E_g reflects the increase in the degree of disorder in the polymer composite.[130,131] Complexes of polar groups of polymeric materials are more likely to form when the extracted tea solution contains enough hydroxyl (OH), carboxylic groups, polyphenols, conjugated double bonds and polyphenol conjugates.[40] The functional groups of Mn–polyphenol complexes then interact as a result of this. The metal complex exhibits a more pronounced reduction in the bandgap compared to other fillers since the polymer chains (PEO) diminish the separation between the valence and conduction bands of the doped polymer material. Has potential applications in optoelectronics. The study's findings demonstrate that the optical dielectric loss spectra as a function of E_{Photon} may be used to estimate the band gap. At the same time, Tauc's model facilitates the identification of the kind of electronic transition.

4.7.2 Cody representations for bandgap study. The model presented by Cody indicates that the optical gap energy of polymer composite films with varying thicknesses can be determined by the cut-cross of the linear extension associated with the spectra that represent $(\alpha/h\nu)^{1/L}$ against E_{Photon} within a constrained range of incident photon energy (the examined range). Tauc assumed that the momentum matrix's component was independent of photon energy, while Cody contends that the dipole matrix element is devoid of photon energy. The calculated optical gap values using Cody's model are displayed in Table 5. Fig. 17(a–d) demonstrates the band energy for the allowed direct and indirect energy gap and the forbidden direct and indirect energy gap, which are derived by crossing this linear extension for the abscissa in accordance with the Cody model of the optical band gap to deduce the optical gap energy.[132] The types of transitions may be seen by contrasting the E_g values in the Cody model (Fig. 17(a–d)) with the energies from the optical dielectric loss (Fig. 16). For PEOMnMC0, it is indirectly permitted ($L = 2$), but for PEOMnMC1, both PEOMnMC2 are directly permitted ($L = 1/2$).

4.7.3 Bandgap analysis by absorption spectrum fitting (ASF) method. Since the valence and conduction band edges are not sharp, the tail states make determining the actual band gap more sophisticated. Accordingly, it is challenging to compute the band gap in amorphous materials rigorously. Therefore, several empirical techniques have been developed to ascertain these materials' band gap. The main advantage of the ASF approach is that it simply requires the absorbance spectrum to be measured; neither the refractive index nor the film thickness is needed.[133] Eqn (9) can be rewritten as a function of wavelength (λ) to introduce the ASF method:

$$\alpha(\lambda) = B(hc)^{m-1}\lambda\left(\frac{1}{\lambda} - \frac{1}{\lambda_g}\right)^L \quad (12)$$

This corresponds to the speed of light (c), Planck's constant (h), and optical gap wavelength (λ_g), respectively. Eqn (2) can be rewritten as follows using Beer–Lambert law:

$$A(\lambda) = D_1\lambda\left(\frac{1}{\lambda} - \frac{1}{\lambda_g}\right)^L + D_2 \quad (13)$$

To the power of $D_1 = [B(hc)^{m-1}d/2.303]$ together with the reflection-affected constant D_2. On top of eqn (13) E_g can be found by fitting the absorbance range. The forbidden optical gap E_{opt}^{ASF} (eV) was estimated by extrapolating the linear segment of at $(A/\lambda)^{1/L} = 0$ from the $(A/\lambda)^{1/L}$ *vs.* $\left(\frac{1}{\lambda}\right)$ curve. Fig. 18(a–d) shows the plot of the current samples for $\left(\frac{A}{\lambda}\right)^2, \left(\frac{A}{\lambda}\right)^{2/3}, \left(\frac{A}{\lambda}\right)^{1/2}, \left(\frac{A}{\lambda}\right)^{1/3}$ *vs.* $\left(\frac{1}{\lambda}\right)$. The least squares method revealed that $L = 2$, 1/2, 2/3, and 1/3 (see Fig. 14). One may find the E_{gap}^{ASF} value in Table 6. Thus, the value of E_g, in eV, can be find from the parameter λ_g using E_{opt}^{ASF} (eV) = 1239.83/λ_g.[134,135] The band gap values computed using the ASF method and derived from Tauc's relation are almost identical. As the

Table 5 The E_g from cady model *versus* photon energy for direct and indirect forbidden and allow transition

Sample code	E_g for $(\alpha/h\nu)^2$	E_g for $(\alpha/h\alpha)^{2/3}$	E_g for $(\alpha/h\alpha)^{1/2}$	E_g for $(\alpha/h\alpha)^{1/3}$
PEOMnMC0	5.6	5.85	5.5	5.7
PEOMnMC1	1.5	1.4	1.25	1.3
PEOMnMC2	1.4	1.1	1.2	1.3

metal complex increases, the band gaps dramatically shrink. These findings suggest that the degree of crystallinity has a significant impact on the optical energy gaps. According to one interpretation of these findings, Localized states in the optical band gap are produced by metal complexes and cause disordered accumulation in the PEO matrix because they are incorporated into the polymer matrix's amorphous region.[136] In comparison between the ASF model and dielectric loss, the results indicate that PEOMnMC0 exhibits direct prohibited characteristics ($L = 3/2$), whereas both PEOMnMC1 and PEOMnMC2 show indirect allowed characteristics ($L = 2$).

The relation provided in eqn (14) can be used to determine the samples' molar refractivity (R_m). The material's molar polarizability (α_m) is closely correlated with R_m.

$$R_m = V_m\left[1 - \sqrt{\frac{E_g}{20}}\right] \quad (14)$$

According to eqn (15), the values of the metallization criterion are entirely dependent on the values of the reflection loss; that is, the higher the reflection loss, the lower the metallization criterion value.

$$M = 1 - R_m/V_m \quad (15)$$

Eqn (14) can be inserted into eqn (15) to obtain eqn (16). The prerequisites for the solid's non-metallic nature are explained by Herzfeld's theory on the metallization of condensed matter. The criteria of metallization Metals are defined by M values near zero, while insulators are described by values near one.[137,138]

$$M = \sqrt{\frac{E_g}{20}} \quad (16)$$

Eqn (16) is an empirical relationship commonly used to assess whether a material exhibits insulating or semiconducting behavior. Specifically, the closer the value of M is to 1, the more insulating the material behaves, and conversely, as M approaches 0, the material demonstrates semiconducting characteristics. Therefore, this relationship is applicable to both insulators and semiconductors. In the context of our polymer composite, the incorporation of the metal complex into the PEO matrix has quantitatively reduced the band gap from (5.5 eV) to (1.4 eV) depending on the concentration of the dopant. As a result of this doping, the M value decreases progressively, approaching zero, indicating a shift toward semiconducting behavior.

By substituting the obtained optical band gap values into eqn (16), the calculated M values are 0.52, 0.274, and 0.264 for PEOMnMC0, PEOMnMC1, and PEOMnMC2, respectively. These values indicate that for pure PEO, M is greater than 0.5 and closer to 1, reflecting predominantly insulating behavior. In contrast, the doped films exhibit M values below 0.5 and closer to 0, suggesting a transition toward semiconducting properties. This means that after doping, the band gap values of the polymer films fall within the typical range for semiconductors. The addition of the metal complex enhances the metallization properties of the composite, as it introduces a significant concentration of metal ions into the polymer matrix, which further contributes to this transition.

4.7.4 Differentiation methods for bandgap estimation. We created a number of additional techniques in this study to determine the bandgap, which is displayed in Fig. 19(a–c). It is worth mentioning that the obtained results from the new models almost match very well with the other standard techniques. There are generally some variations between the approaches, possibly as a result of tiny variations in line calculation and smoothing during sketching the graphs. Plotting the first derivative of transmittance spectra as a function of E_{Photon} is the basis for the first two of four approaches used to calculate E_g. Fig. 19(a and b) displays the derivative of transmittance $dT/d\lambda$, $dR/d\lambda$, the optical reflectance's first derivative. These techniques calculate the gap's energy from the initial greatest peak in the upper range of x-axis energies. Table 7 confirms the optical bandgap value and displays the values for undoped and PEO composite, $dT/d\lambda$ and $dR/d\lambda$. The absorption edge, donor carrier concentration, and impurity energy levels all have a direct impact on the optical bandgap's variance. This leads to an increase in the degree of defects, which are represented by the Urbach energy, and ultimately, a drop in the gap energy. Furthermore, as shown in Fig. 19(c), $dn/d\lambda$ has a negative component that represents the bandgap at each curve's greatest peak.[139,140] By comparing three differentiation methods for studying the band gap for all composite samples with dielectric loss, we see that $dT/d\lambda$ it is a remarkable way to study the band gap for both PEOMnMC0 and PEOMnMC1 but ($dR/d\lambda$, $dn/d\lambda$) is notable for PEOMnMC2.

4.8. Urbach energy (E_u) study

Urbach energy, also known as Urbach tail, is regarded as a reliable and significant tool for investigating the structural characteristics of polymeric materials. It enables us to determine and characterize the defect levels within these materials' band gap.[93] Moreover, understanding the E_u found in disordered

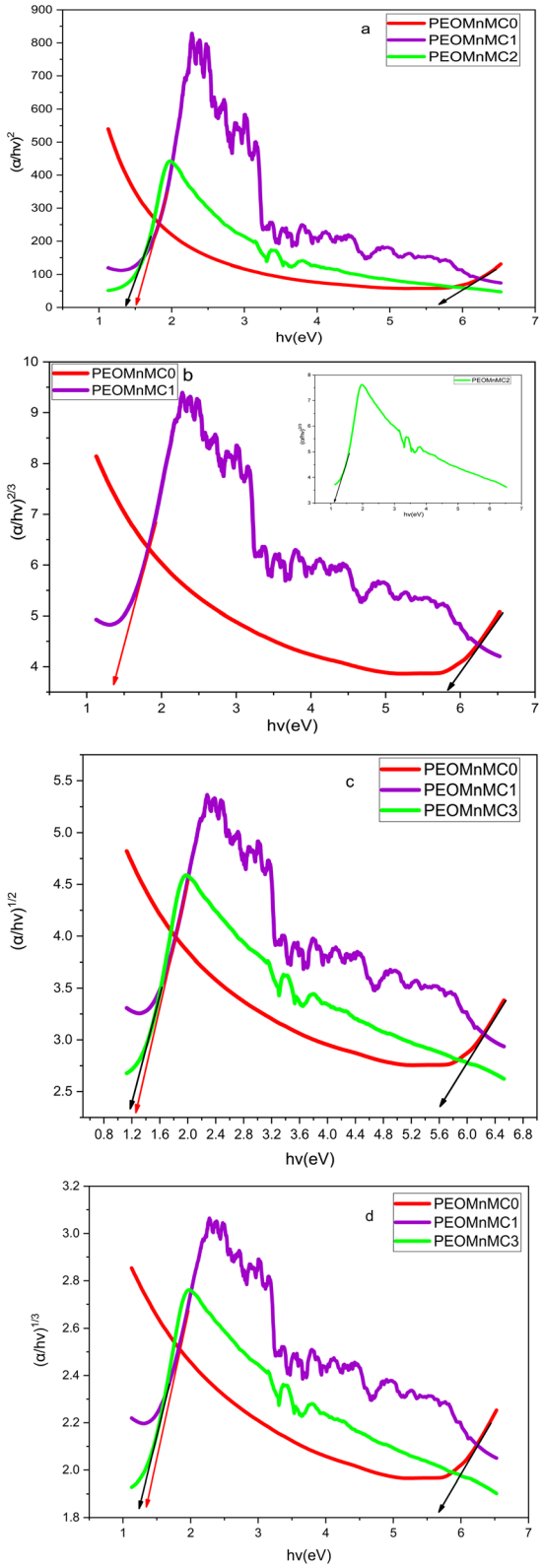

Fig. 17 (a–d) Plots the correlation between the undoped and modified PEO, E_{Photon}, with $(\alpha/h\nu)^{1/L}$.

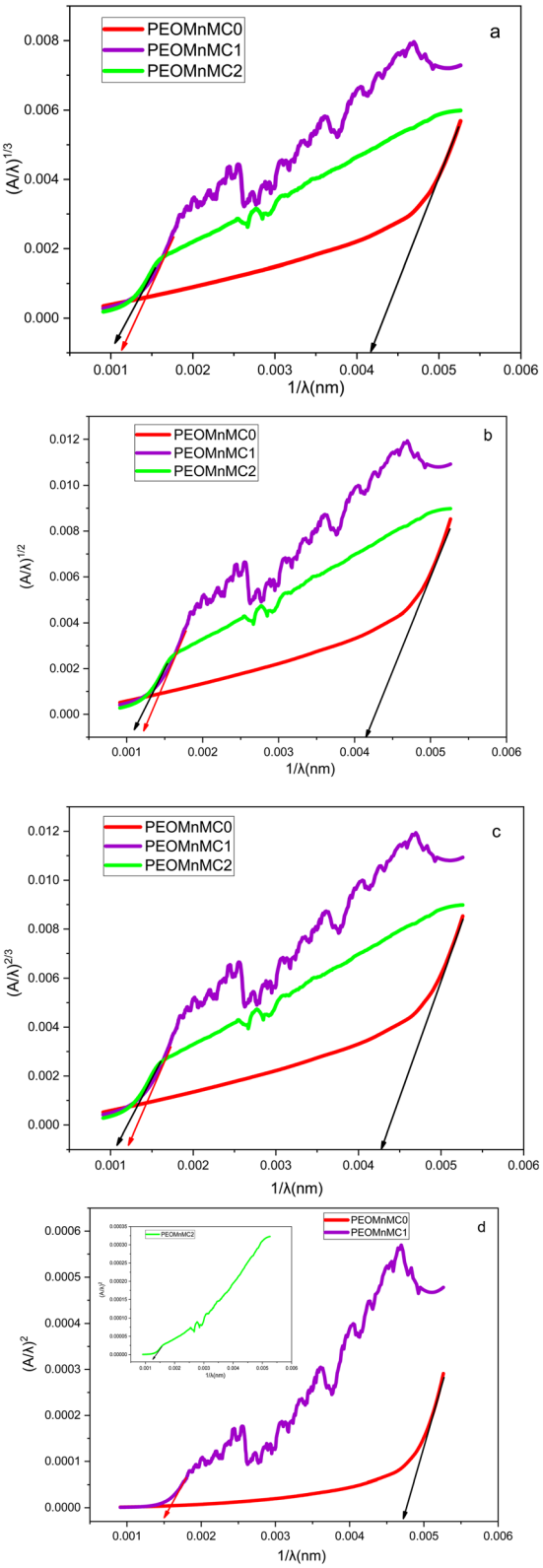

Fig. 18 (a–d) The connection between $(A/\lambda)^{1/w}$ and E_{Photon} for both undoped and modified PEO composites using the ASF approach.

materials is crucial to comprehending their electronic transport characteristics. It is known that strains in the network that are strong enough to force the states into the forbidden gap are the source of band tail states in amorphous materials. In the gap, such tails decay exponentially. Which subtly suggests that the polymers are becoming more amorphous.[141] The following

Table 6 The E_g from ASF method *versus* photon energy for direct and indirect forbidden and allow transition

	$L = 2$		$L = 3/2$		$L = 1/2$		$L = 3$	
Sample	λ_g	E_{OP}^{ASF}	λ_g	E_{OP}^{ASF}	λ_g	E_{OP}^{ASF}	λ_g	E_{OP}^{ASF}
PEOMnMC0	238.095	5.207	232.558	5.3313	212.766	5.827	238.095	5.207
PEOMnMC1	833.333	1.488	819.672	1.513	666.667	1.859	909.091	1.364
PEOMnMC2	909.091	1.364	952.381	1.302	800	1.549	1000	1.239

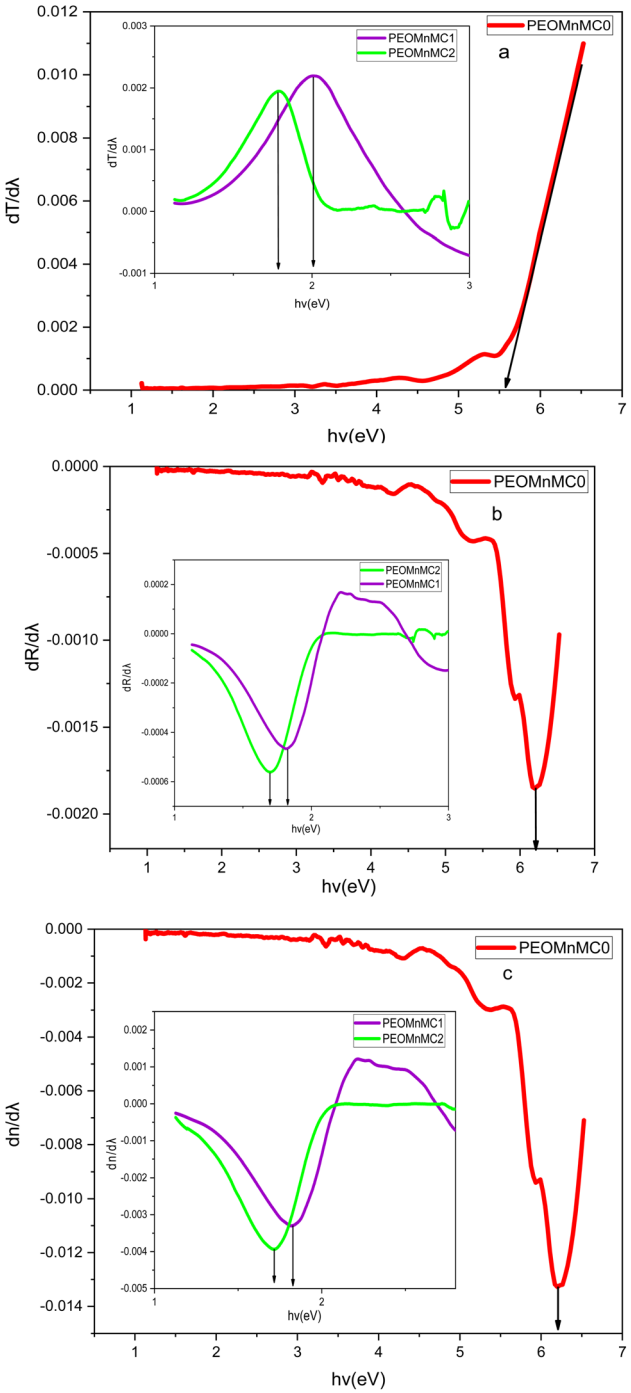

Fig. 19 (a–c) (a) $dT/d\lambda$, (b) $dR/d\lambda$, (c) $dn/d\lambda$ with E_{Photon} for finding E_g of undoped and modified PEO.

empirical relation was used to calculate the width of Urbach energy.[142]

$$\alpha = \alpha_0 \exp^{h\nu/E_u} \quad (17)$$

where (E_u) is the average width of the band tails of the localized regions in the films and $\alpha_0$is a constant. Fig. 20 displays the relation between ln(α) and $h\nu$ for pure and doped PEO. The straight lines showed that the absorption complies with the Urbach rule and the quadratic relation for inter-band transition. Table 1 displays the band tail E_u values, which were determined by taking the reciprocal of these lines' slopes.

It is evident that the Urbach energy rises from 1.34 to 1.61 as the concentration of metal complexes increases. This subtly suggests that polymer composite samples have a more amorphous phase.[142] The composites' band structure will become disordered and imperfect due to the larger energy tails. According to this observation, more localized states were produced within the forbidden energy gap as well. In contrast,

Table 7 Different methods to investigate the optical band gap E_g (eV) and comparison between them

Sample	$dT/d\lambda$	$dR/d\lambda$	$dn/d\lambda$
PEOMnMC0	5.55	6.3	6.3
PEOMnMC1	2	1.8	1.8
PEOMnMC2	1.8	1.7	1.7

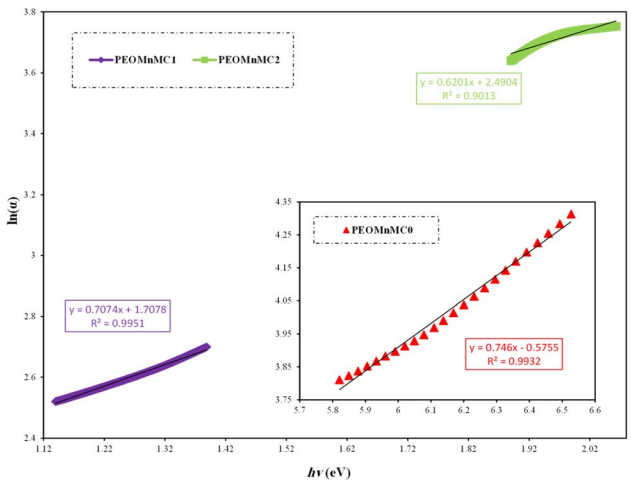

Fig. 20 Plot of ln(α) as a function of E_{Photon} for the pure and modified PEO film.

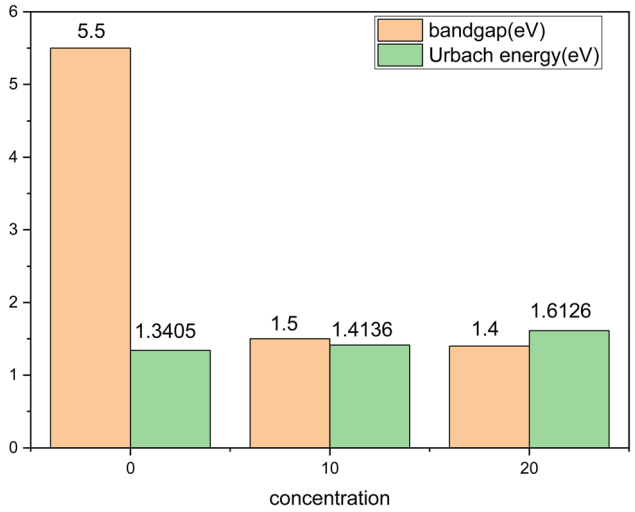

Fig. 21 At different concentrations, there is a correlation between the E_g and the Urbach energy of undoped and modified PEO.

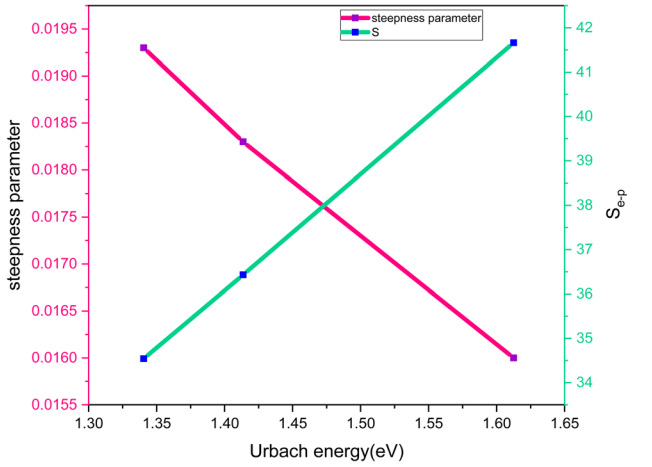

Fig. 22 Correlation between the steepness parameter and electron–phonon interaction as a function of Urbach energy.

PEO had a smaller energy tail width, which is directly related to its neat polymer structure and, consequently, its larger energy gap.[143] The relationship between undoped and modified PEO films at different concentrations of metal complexes is shown in Fig. 21. It is evident that the polymer's bandgap reaches its minimum value, and the Urbach energy reaches its maximum as the metal complex concentration rises. The presence of localized defect states in the bandgap energy around the valence band maximum and conduction band minimum easily explains the decrease of the bandgap in polymer composites of thin films. The disorder in the composite film increased due to a localized condition in the material, which raised the Urbach energy.[144–146]

Furthermore, by determining the electron–phonon interaction strength (S_{e-p}) and the steepness parameter (β), (β) represents a novel optical constant. This parameter denotes the slope or gradient of the linear section of the absorption curve adjacent to the absorption edge, which regulates the rate of energy variation. The subsequent description pertains to the evaluation of the values of (β).[147]

$$\beta = \frac{k_B T}{E_u} \quad (18)$$

k_B, is equal to 8.6173×10^{-5} eV K^{-1}, where T is the ambient temperature (300 K). β is related also to the strength of the electron–phonon interaction (S_{e-p}) by the following relationship.[148]

$$S_{e-p} = 2/3\beta \quad (19)$$

This parameter describes the lattice expanding and increasing of the lattice constants.[146] Fig. 22 illustrates the correlation between the steepness parameter and the magnitude of the electron–phonon interaction with respect to the Urbach energy. As disorder develops, the electron–phonon interaction grows due to reduced atomic spacing, resulting in larger absorption spectra, and the bandgap may decrease owing to phonon scattering. However, the steepness of the energy fluctuation diminishes, which results in a lower slope, indicating that absorption shifts to the higher wavelength. This is frequently linked to disorder or localized states within the material, which is essential for optoelectronic applications such as solar cells, sensors, and photovoltaics.

5. Conclusion

This study successfully demonstrated the fabrication of PEO-based polymer composites doped with manganese–polyphenol complexes synthesized using black tea extract *via* a green chemistry route. The structural and optical analyses confirmed that the incorporation of the Mn–polyphenol complex significantly modified the crystallinity, morphology, and electronic properties of the PEO matrix. FTIR spectra revealed a strong interaction between the polyphenolic compounds and Mn(II) ions, forming stable metal–ligand coordination complexes. XRD analysis showed a reduction in crystallinity and increased amorphous behavior with higher concentrations of the Mn–polyphenol complex. The OM micrographs of PEO films indicate that crystallinity diminishes as the concentration of Mn–polyphenol increases. The spherulite structure disintegrates into smaller entities, resulting in black patches on the polymer film surface, which signifies the promotion of the amorphous phase. UV-visible spectroscopy indicated that the composites exhibit tunable optical properties, including a decrease in band gap and a shift in absorption edge toward lower photon energy with increasing complex content. Various models such as absorption coefficient, Taucs model, optical dielectric loss and ASF approach were successfully used to evaluate the optical band gap. The optical bandgap narrowed from approximately 5.5 eV in pure PEO to 1.4 eV in the doped samples, as supported by Taucs analysis and dielectric measurements. The green synthesis approach using black tea extract proved to be effective, eco-friendly, and capable of producing functional polymer composites with potential applications in optoelectronics and photonics.

Data availability

The data supporting the findings of this study are available from the corresponding authors upon reasonable request. This includes the raw data from XRD, FTIR, and UV-vis spectroscopy analyses, as well as the processed datasets used for calculating optical properties such as bandgap, Urbach energy, and dielectric loss. All relevant materials and methods used for data collection and analysis are described in the manuscript.

Conflicts of interest

There are no conflicts to declare.

References

1 M. G. Kiran, *et al.*, Studies on optical properties of Pva based complex polymer electrolyte, *Rasayan J. Chem.*, 2021, **14**, 760–767.
2 D. S. Muhammed, *et al.*, Optical dielectric loss as a novel approach to specify the types of electron transition: XRD and UV-vis as a non-destructive techniques for structural and optical characterization of PEO based nanocomposites, *Materials*, 2020, **13**(13), 2979.
3 H. T. Ahmed and O. G. Abdullah, Preparation and composition optimization of PEO: MC polymer blend films to enhance electrical conductivity, *Polymers*, 2019, **11**(5), 853.
4 A. Alias, *et al.*, Optical characterization and properties of polymeric materials for optoelectronic and photonic applications, *Int. J. Appl. Sci. Technol.*, 2013, **3**(5), 11–38.
5 S. Ramesh, *et al.*, Preparation and characterization of plasticized high molecular weight PVC-based polymer electrolytes, *Sadhana*, 2010, **35**, 87–95.
6 A. M. Alsaad, *et al.*, The structural, optical, thermal, and electrical properties of synthesized PEO/GO thin films, *Appl. Phys. A*, 2022, **128**(8), 676.
7 O. G. Abdullah and S. A. Hussen, Variation of optical band gap width of PVA films doped with aluminum iodide, *Adv. Mater. Res.*, 2012, **383**, 3257–3263.
8 M. El-Mansy, *et al.*, Characterization of PVA/CuI polymer composites as electron donor for photovoltaic application, *Optik*, 2013, **124**(13), 1624–1631.
9 O. G. Abdullah, *et al.*, Optical properties of PVA: CdCl2. H2O polymer electrolytes, *IOSR J. Appl. Phys.*, 2013, **4**(3), 52–57.
10 V. Mohan, *et al.*, Optical and electrical properties of pure and doped PEO polymer electrolyte films, *Soft Mater.*, 2007, **5**(1), 33–46.
11 K. K. Ahmed, *et al.*, A brief review on optical properties of polymer Composites: Insights into light-matter interaction from classical to quantum transport point of view, *Results Phys.*, 2023, 107239.
12 S. B. Aziz, *et al.*, Tuning the absorption of ultraviolet spectra and optical parameters of aluminum doped PVA based solid polymer composites, *J. Mater. Sci.: Mater. Electron.*, 2015, **26**, 8022–8028.
13 M. Brza, *et al.*, Green coordination chemistry as a novel approach to fabricate polymer: Cd (II)-complex composites: Structural and optical properties, *Opt. Mater.*, 2021, **116**, 111062.
14 P. A. Mohammed, *et al.*, Self-supported light induced polymer waveguide for thin optical fiber interconnection, *Opt. Fiber Technol.*, 2022, **68**, 102792.
15 P. A. Mohammed, Integration of knee-shaped self-written waveguides between optical fibers by direct illumination and tip to tip coupling, *Opt. Mater.*, 2024, **147**, 114713.
16 P. A. Mohammed, Optical and mechanical properties of self-written polymer waveguide between single mode optical fibers using UV photocurable monomer system, *Eur. Polym. J.*, 2020, **139**, 109950.
17 K. K. Ahmed, S. A. Hussen and S. B. Aziz, Transferring the wide band gap chitosan: POZ-based polymer blends to small optical energy band gap polymer composites through the inclusion of green synthesized Zn2+-PPL metal complex, *Arab. J. Chem.*, 2022, **15**(7), 103913.
18 I. A. Ahmed, *et al.*, Green synthesis of Fe–Cu bimetallic supported on alginate-limestone nanocomposite for the removal of drugs from contaminated water, *Polymers*, 2023, **15**(5), 1221.
19 K. K. Ahmed, *et al.*, A brief review on optical properties of polymer composites: insights into light-matter interaction from classical to quantum transport point of view, *Results Phys.*, 2024, **56**, 107239.
20 R. Bharti and R. Sharma, Effect of heavy metals: An overview, *Mater. Today: Proc.*, 2022, **51**, 880–885.
21 Y. Y. Loo, *et al.*, Synthesis of silver nanoparticles by using tea leaf extract from Camellia sinensis, *Int. J. Nanomed.*, 2012, 4263–4267.
22 D. Q. Muheddin, S. B. Aziz and P. A. Mohammed, Variation in the optical properties of PEO-based composites via a green metal complex: macroscopic measurements to explain microscopic quantum transport from the valence band to the conduction band, *Polymers*, 2023, **15**(3), 771.
23 P. Kouvaris, *et al.*, Green synthesis and characterization of silver nanoparticles produced using Arbutus unedo leaf extract, *Mater. Lett.*, 2012, **76**, 18–20.
24 J. W. Drynan, *et al.*, The chemistry of low molecular weight black tea polyphenols, *Nat. Prod. Rep.*, 2010, **27**(3), 417–462.
25 L. Wang, *et al.*, Impact of Kombucha Fermentation on the Flavor and Physicochemical Properties of Tea (Camellia sinensis) Flower Infusions, *Food Front.*, 2025, **6**(2), 750–762.
26 M. Brza, *et al.*, Tea from the drinking to the synthesis of metal complexes and fabrication of PVA based polymer composites with controlled optical band gap, *Sci. Rep.*, 2020, **10**(1), 18108.
27 M. Zdenka, *et al.*, Iron (II, III)–Polyphenol Complex Nanoparticles Derived from Green Tea with Remarkable Ecotoxicological Impact, *ACS Sustainable Chem. Eng.*, 2014, **2**(7), 1674–1680.
28 Z. Wang, Iron complex nanoparticles synthesized by eucalyptus leaves, *ACS Sustain. Chem. Eng.*, 2013, **1**(12), 1551–1554.

29 M. Brza, *et al.*, From green remediation to polymer hybrid fabrication with improved optical band gaps, *Int. J. Mol. Sci.*, 2019, **20**(16), 3910.
30 D. S. Muhammad, D. M. Aziz and S. B. Aziz, The impact of green chemistry to synthesize PVA/cobalt metal complexes (CoMCs) composites with enhanced optical behavior, *Opt. Mater.*, 2025, **158**, 116448.
31 S. B. Aziz, *et al.*, Innovative green chemistry approach to synthesis of Sn2+-metal complex and design of polymer composites with small optical band gaps, *Molecules*, 2022, **27**(6), 1965.
32 H. M. Ahmad, S. H. Sabeeh and S. A. Hussen, Electrical and optical properties of PVA/LiI polymer electrolyte films, *Asian Trans. Sci. Technol.*, 2012, **1**(6), 16–20.
33 H. K. Koduru, N. Scaramuzza and Y. Marinov, Optical properties of multi-layers structured PEO/PVP solid polymer membranes doped with sodium perchlorate, *J. Phys.: Conf. Ser.*, 2023, 012026.
34 S. B. Aziz, *et al.*, Optical properties of pure and doped PVA: PEO based solid polymer blend electrolytes: two methods for band gap study, *J. Mater. Sci.: Mater. Electron.*, 2017, **28**, 7473–7479.
35 A. Hadi, A. Hashim and Y. Al-Khafaji, Structural, optical and electrical properties of PVA/PEO/SnO2 new nanocomposites for flexible devices, *Trans. Electr. Electron. Mater.*, 2020, **21**(3), 283–292.
36 K. Abdali, *et al.*, Morphological, Optical, ElectricalCharacterizations and Anti-Escherichia coli Bacterial Efficiency (AECBE) of PVA/PAAm/PEO Polymer Blend Doped with Silver NPs, *Nano Biomed. Eng.*, 2022, **14**(2), 114–122.
37 R. M. Abdullah, *et al.*, Reducing the crystallite size of spherulites in PEO-based polymer nanocomposites mediated by carbon nanodots and Ag nanoparticles, *Nanomaterials*, 2019, **9**(6), 874.
38 E. M. Abdelrazek, *et al.*, Structural, optical, morphological and thermal properties of PEO/PVP blend containing different concentrations of biosynthesized Au nanoparticles, *J. Mater. Res. Technol.*, 2018, **7**(4), 419–431.
39 S. B. Aziz, *et al.*, Characteristics of PEO incorporated with CaTiO3 nanoparticles: structural and optical properties, *Polymers*, 2021, **13**(20), 3484.
40 S. B. Aziz, Modifying poly (vinyl alcohol)(PVA) from insulator to small-bandgap polymer: A novel approach for organic solar cells and optoelectronic devices, *J. Electron. Mater.*, 2016, **45**(1), 736–745.
41 S. B. Aziz, *et al.*, From insulating PMMA polymer to conjugated double bond behavior: Green chemistry as a novel approach to fabricate small band gap polymers, *Polymers*, 2017, **9**(11), 626.
42 M. Atta, *et al.*, Structural, optical, and thermal properties of PEO/PVP blend reinforced biochar, *Opt. Mater.*, 2022, **127**, 112268.
43 S. Aziz, *et al.*, Structural, thermal, morphological and optical properties of PEO filled with biosynthesized Ag nanoparticles: new insights to band gap study, *Results Phys.*, 2019, **13**, 102220.
44 S. Khokhar and R. K. O. Apenten, Iron binding characteristics of phenolic compounds: some tentative structure–activity relations, *Food Chem.*, 2003, **81**(1), 133–140.
45 M. Spiegel, K. Cel and Z. Sroka, The mechanistic insights into the role of pH and solvent on antiradical and prooxidant properties of polyphenols—Nine compounds case study, *Food Chem.*, 2023, **407**, 134677.
46 H. Hassan, *et al.*, Trivalent metal complexes of Rich-Hyrdoxy Schiff base ligand: synthesis, characterization, DFT calculations and antimicrobial activity, *J. Zankoy Sulaimani, Part A*, 2023, **25**(2), 25.
47 L. Mira, *et al.*, Interactions of flavonoids with iron and copper ions: a mechanism for their antioxidant activity, *Free Radic. Res.*, 2002, **36**(11), 1199–1208.
48 N. Salleh, *et al.*, Electrical impedance and conduction mechanism analysis of biopolymer electrolytes based on methyl cellulose doped with ammonium iodide, *Ionics*, 2016, **22**, 2157–2167.
49 Z. Wang and P. An, Characterization of copper complex nanoparticles synthesized by plant polyphenols, *bioRxiv*, 2017, 134940.
50 Z. Wang, C. Fang and M. Mallavarapu, Characterization of iron–polyphenol complex nanoparticles synthesized by Sage (Salvia officinalis) leaves, *Environ. Technol. Innovat.*, 2015, **4**, 92–97.
51 R. Yang, *et al.*, Electrical properties of composite polymer electrolytes based on PEO-SN-LiCF3SO3, *Int. J. Electrochem. Sci.*, 2013, **8**(8), 10163–10169.
52 A. Rajeh, M. Morsi and I. Elashmawi, Enhancement of spectroscopic, thermal, electrical and morphological properties of polyethylene oxide/carboxymethyl cellulose blends: combined FT-IR/DFT, *Vacuum*, 2019, **159**, 430–440.
53 S. B. Aziz, *et al.*, Structural, thermal, morphological and optical properties of PEO filled with biosynthesized Ag nanoparticles: New insights to band gap study, *Results Phys.*, 2019, **13**, 102220.
54 S. B. Aziz and Z. H. Z. Abidin, Ion-transport study in nanocomposite solid polymer electrolytes based on chitosan: electrical and dielectric analysis, *J. Appl. Polym. Sci.*, 2015, **132**(15), 41774.
55 S. B. Aziz and R. M. Abdullah, Crystalline and amorphous phase identification from the tanδ relaxation peaks and impedance plots in polymer blend electrolytes based on [CS: AgNt] x: PEO (x-1)(10≤ x≤ 50), *Electrochim. Acta*, 2018, **285**, 30–46.
56 P. K. Singh, K.-W. Kim and H.-W. Rhee, Electrical, optical and photoelectrochemical studies on a solid PEO-polymer electrolyte doped with low viscosity ionic liquid, *Electrochem. Commun.*, 2008, **10**(11), 1769–1772.
57 S. B. Aziz, M. Faraj and O. G. Abdullah, Impedance spectroscopy as a novel approach to probe the phase transition and microstructures existing in CS: PEO based blend electrolytes, *Sci. Rep.*, 2018, **8**(1), 14308.
58 A. Karmakar and A. Ghosh, Poly ethylene oxide (PEO)–LiI polymer electrolytes embedded with CdO nanoparticles, *J. Nanopart. Res.*, 2011, **13**, 2989–2996.

59 M. Marzantowicz, *et al.*, Crystallization and melting of PEO: LiTFSI polymer electrolytes investigated simultaneously by impedance spectroscopy and polarizing microscopy, *Electrochim. Acta*, 2005, **50**(19), 3969–3977.
60 T. Bandara, *et al.*, Electrical and complex dielectric behaviour of composite polymer electrolyte based on PEO, alumina and tetrapropylammonium iodide, *Ionics*, 2017, **23**, 1711–1719.
61 B. Y. Ahmed and S. O. Rashid, Synthesis, characterization, and application of metal-free sulfonamide-vitamin C adduct to improve the optical properties of PVA polymer, *Arab. J. Chem.*, 2022, **15**(10), 104096.
62 A. Szymczycha-Madeja, M. Welna and W. Zyrnicki, Multi-element analysis, bioavailability and fractionation of herbal tea products, *J. Braz. Chem. Soc.*, 2013, **24**, 777–787.
63 J. M. Hadi, *et al.*, Investigation of ion transport parameters and electrochemical performance of plasticized biocompatible chitosan-based proton conducting polymer composite electrolytes, *Membranes*, 2020, **10**(11), 363.
64 S. B. Aziz, *et al.*, A comprehensive review on optical properties of polymer electrolytes and composites, *Materials*, 2020, **13**(17), 3675.
65 S. P. Dubey, M. Sillanpaa and R. S. Varma, Reduction of hexavalent chromium using Sorbaria sorbifolia aqueous leaf extract, *Appl. Sci.*, 2017, **7**(7), 715.
66 S. Senthilkumar and T. Sivakumar, Green tea (Camellia sinensis) mediated synthesis of zinc oxide (ZnO) nanoparticles and studies on their antimicrobial activities, *Int. J. Res. Pharm. Sci.*, 2014, **6**(6), 461–465.
67 L. M. Quintero-Borregales, *et al.*, Black tea extracts/polyvinyl alcohol active nanofibers electrospun mats with sustained release of polyphenols for food packaging applications, *Polymers*, 2023, **15**(5), 1311.
68 L. Huang, *et al.*, Synthesis of iron-based nanoparticles using oolong tea extract for the degradation of malachite green, *Spectrochim. Acta, Part A*, 2014, **117**, 801–804.
69 H. Zhou, *et al.*, Discrimination of tea varieties based on FTIR spectroscopy and an adaptive improved possibilistic c-means clustering, *J. Food Process. Preserv.*, 2020, **44**(10), e14795.
70 D. Wu and M. R. Bird, The interaction of protein and polyphenol species in ready to drink black tea liquor production, *J. Food Process. Eng.*, 2010, **33**(3), 481–505.
71 Z. Markova, *et al.*, Iron (II, III)–polyphenol complex nanoparticles derived from green tea with remarkable ecotoxicological impact, *ACS Sustain. Chem. Eng.*, 2014, **2**(7), 1674–1680.
72 M. M. Nofal, *et al.*, Polymer composites with 0.98 transparencies and small optical energy band gap using a promising green methodology: Structural and optical properties, *Polymers*, 2021, **13**(10), 1648.
73 S. B. Aziz, *et al.*, Characteristics of poly (Vinyl alcohol)(PVA) based composites integrated with green synthesized Al3+-metal complex: Structural, optical, and localized density of state analysis, *Polymers*, 2021, **13**(8), 1316.
74 M. Brza, *et al.*, Electrochemical impedance spectroscopy as a novel approach to investigate the influence of metal complexes on electrical properties of Poly (vinyl alcohol)(PVA) composites, *Int. J. Electrochem. Sci.*, 2021, **16**(5), 210542.
75 S. Kilarkaje, V. Manjunatha and H. Devendrappa, Optical and electrical characterization of (PEO+ methyl violet) polymer electrolytes, *J. Appl. Polym. Sci.*, 2012, **124**(3), 2558–2566.
76 S. Ramesh, T. F. Yuen and C. J. Shen, Conductivity and FTIR studies on PEO–LiX [X: CF3SO3−, SO42−] polymer electrolytes, *Spectrochim. Acta, Part A*, 2008, **69**(2), 670–675.
77 P. P. Chu, M. J. Reddy and J. Tsai, Structural and transport characteristics of polyethylene oxide/phenolic resin blend solid polymer electrolytes, *J. Polym. Sci., Part B: Polym. Phys.*, 2004, **42**(21), 3866–3875.
78 S. Patil, S. Yawale and S. Yawale, Conductivity study of PEO-LiClO4 polymer electrolyte doped with ZnO nanocomposite ceramic filler, *Bull. Mater. Sci.*, 2014, **37**(6), 1403–1409.
79 L. Senak, M. A. Davies and R. Mendelsohn, A quantitative IR study of hydrocarbon chain conformation in alkanes and phospholipids: CH2 wagging modes in disordered bilayer and HII phases, *J. Phys. Chem.*, 1991, **95**(6), 2565–2571.
80 N. Sudharshan and V. Swetha, UV-Visible Spectroscopy: A Comprehensive Review On Instrumentation, *Int. J. All Res. Educ. Sci. Methods*, 2023, **12**(1), 1501–1507.
81 R. Kumar, *et al.*, Study of optical band gap and carbonaceous clusters in swift heavy ion irradiated polymers with UV–Vis spectroscopy, *Nucl. Instrum. Methods Phys. Res., Sect. B*, 2008, **266**(8), 1788–1792.
82 M. Reto, *et al.*, Chemical composition of green tea (Camellia sinensis) infusions commercialized in Portugal, *Plant Foods Hum. Nutr.*, 2007, **62**, 139–144.
83 A. Sanaeifar, *et al.*, Nondestructive monitoring of polyphenols and caffeine during green tea processing using Vis-NIR spectroscopy, *Nutr. Food Sci.*, 2020, **8**(11), 5860–5874.
84 S. Ibrahim, R. Ahmad and M. R. Johan, Conductivity and optical studies of plasticized solid polymer electrolytes doped with carbon nanotube, *J. Lumin.*, 2012, **132**(1), 147–152.
85 Z. Wang, C. Fang and M. Megharaj, Characterization of iron–polyphenol nanoparticles synthesized by three plant extracts and their fenton oxidation of azo dye, *ACS Sustain. Chem. Eng.*, 2014, **2**(4), 1022–1025.
86 X. Wang, *et al.*, Identification of green tea varieties and fast quantification of total polyphenols by near-infrared spectroscopy and ultraviolet-visible spectroscopy with chemometric algorithms, *Anal. Methods*, 2015, **7**(2), 787–792.
87 A. Gani, *et al.*, Time-dependent extraction kinetics of infused components of different Indian black tea types using UV spectroscopy, *Cogent Food Agric.*, 2016, **2**(1), 1137157.
88 L. Zhang, *et al.*, *Characterization of Black Tea Stems and Leaves Using Multiple-Spectral Analysis of 1h Nmr, Uv-Vis, and Ftir Coupled with Multivariate Statistics. Uv-Vis, and Ftir Coupled with Multivariate Statistics*.

89 P. K. Jain, *et al.*, Surface plasmon resonance enhanced magneto-optics (SuPREMO): Faraday rotation enhancement in gold-coated iron oxide nanocrystals, *Nano Lett.*, 2009, **9**(4), 1644–1650.
90 S. B. Aziz, *et al.*, Improving EDLC device performance constructed from plasticized magnesium ion conducting chitosan based polymer electrolytes via metal complex dispersion, *Membranes*, 2021, **11**(4), 289.
91 S. B. Aziz, Morphological and optical characteristics of chitosan (1−x): Cuo x (4≤ x≤ 12) based polymer nanocomposites: Optical dielectric loss as an alternative method for tauc's model, *Nanomaterials*, 2017, **7**(12), 444.
92 S. B. Aziz, *et al.*, Polymer blending as a novel approach for tuning the SPR peaks of silver nanoparticles, *Polymers*, 2017, **9**(10), 486.
93 D. M. Aziz, *et al.*, Spectroscopic study of wemple-didomenico empirical formula and taucs model to determine the optical band gap of dye-doped polymer based on chitosan: Common poppy dye as a novel approach to reduce the optical band gap of biopolymer, *Spectrochim. Acta, Part A*, 2025, **325**, 125142.
94 D. S. Muhammad, D. M. Aziz and S. B. Aziz, Zinc metal complexes synthesized by a green method as a new approach to alter the structural and optical characteristics of PVA: new field for polymer composite fabrication with controlled optical band gap, *RSC Adv.*, 2024, **14**(36), 26362–26387.
95 H. Xu, *et al.*, Recent progress in metal–organic complexes for optoelectronic applications, *Chem. Soc. Rev.*, 2014, **43**(10), 3259–3302.
96 R. T. Abdulwahid, *et al.*, The study of structural and optical properties of PVA: PbO 2 based solid polymer nanocomposites, *J. Mater. Sci.: Mater. Electron.*, 2016, **27**, 12112–12118.
97 F. B. Koyuncu, *et al.*, A new low band gap electrochromic polymer containing 2, 5-bis-dithienyl-1H-pyrrole and 2, 1, 3-benzoselenadiazole moiety with high contrast ratio, *Polymer*, 2011, **52**(25), 5772–5779.
98 T. S. Soliman, *et al.*, Investigation of linear optical parameters and dielectric properties of polyvinyl alcohol/ZnO nanocomposite films, *Phys. Status Solidi A*, 2020, **217**(19), 2000321.
99 S. B. Aziz, *et al.*, Green Chemistry Approach to Decline the Optical Band Gap of MC Polymer Using Hollyhock Natural Dye, *J. Inorg. Organomet. Polym. Mater.*, 2024, 1–17.
100 F. Yakuphanoglu and M. Arslan, The fundamental absorption edge and optical constants of some charge transfer compounds, *Opt. Mater.*, 2004, **27**(1), 29–37.
101 A. Edukondalu, *et al.*, Optical properties of amorphous Li2O–WO3–B2O3 thin films deposited by electron beam evaporation, *J. Taibah Univ. Sci.*, 2016, **10**(3), 363–368.
102 S. A. Mohamed, *et al.*, Effect of ethylene carbonate as a plasticizer on CuI/PVA nanocomposite: Structure, optical and electrical properties, *J. Adv. Res.*, 2014, **5**(1), 79–86.
103 S. B. Aziz, *et al.*, Structural and optical characteristics of pva: C-dot composites: Tuning the absorption of ultra violet (uv) region, *Nanomaterials*, 2019, **9**(2), 216.
104 P. B. Bhargav, *et al.*, Structural, electrical and optical characterization of pure and doped poly (vinyl alcohol)(PVA) polymer electrolyte films, *Int. J. Polym. Mater.*, 2007, **56**(6), 579–591.
105 S. B. Aziz, M. A. Rasheed and Z. H. Abidin, Optical and electrical characteristics of silver ion conducting nanocomposite solid polymer electrolytes based on chitosan, *J. Electron. Mater.*, 2017, **46**, 6119–6130.
106 O. G. Abdullah, S. B. Aziz and M. A. Rasheed, Effect of silicon powder on the optical characterization of Poly (methyl methacrylate) polymer composites, *J. Mater. Sci.: Mater. Electron.*, 2017, **28**, 4513–4520.
107 G. Mohammed, A. M. El Sayed and W. Morsi, Spectroscopic, thermal, and electrical properties of MgO/polyvinyl pyrrolidone/polyvinyl alcohol nanocomposites, *J. Phys. Chem. Solids*, 2018, **115**, 238–247.
108 C. Li, *Refractive Index Engineering and Optical Properties Enhancement by Polymer Nanocomposites*, 2016.
109 K. Jameel Tahir and R. Al-Yasari, Structural and Optical Properties of polyvinyl alcohol doped silver (PVA: Ag) film, *J. Nanostruct.*, 2018, **8**(4), 359–365.
110 E. A. Costner, *et al.*, Fundamental optical properties of linear and cyclic alkanes: VUV absorbance and index of refraction, *J. Phys. Chem. A*, 2009, **113**(33), 9337–9347.
111 H. M. Alghamdi and A. Rajeh, Synthesis and improved optical, electrical, and dielectric properties of PEO/PVA/CuCo2O4 nanocomposites, *Sci. Rep.*, 2024, **14**(1), 18925.
112 T. Soliman, S. Vshivkov and S. I. Elkalashy, Structural, linear and nonlinear optical properties of Ni nanoparticles–Polyvinyl alcohol nanocomposite films for optoelectronic applications, *Opt. Mater.*, 2020, **107**, 110037.
113 S. Divya, *et al.*, Evaluation of nonlinear optical parameters of TiN/PVA nanocomposite–A comparison between semi empirical relation and Z-Scan results, *Curr. Appl. Phys.*, 2014, **14**(1), 93–98.
114 P. Singh and R. Kumar, Investigation of refractive index dispersion parameters of Er doped ZnO thin films by WDD model, *Optik*, 2021, **246**, 167829.
115 A. M. Nawar, M. Mohammed and I. Yahia, Facile synthesis and optical characterization of graphene oxide-doped TiO2/polyvinyl alcohol nanocomposites: optical limiting applications, *Mater. Res. Express*, 2019, **6**(7), 075054.
116 W. Spitzer and H. Fan, Determination of optical constants and carrier effective mass of semiconductors, *Phys. Rev.*, 1957, **106**(5), 882.
117 E. K. Shokr, *et al.*, Optical characterizations of lightly doped (PbS) 1− x Zn x thin films influenced by film thickness and annealing temperature for applications in highly intensive radiation systems, *J. Mater. Sci.: Mater. Electron.*, 2023, **34**(28), 1929.
118 A. M. Abd-Elnaiem, *et al.*, Substituting silver for tellurium in selenium–tellurium thin films for improving the optical characteristics, *J. Inorg. Organomet. Polym. Mater.*, 2022, **32**(6), 2009–2021.

119 M. F. Al-Mudhaffer, M. A. Nattiq and M. A. Jaber, Linear optical properties and energy loss function of Novolac: epoxy blend film, *Arch. Appl. Sci. Res.*, 2012, **4**(4), 1731–7140.
120 S. B. Aziz, *et al.*, Fabrication of polymer blend composites based on [PVA-PVP](1−x):(Ag2S) x (0.01≤ x≤ 0.03) with small optical band gaps: Structural and optical properties, *Mater. Sci. Semicond. Process.*, 2017, **71**, 197–203.
121 M. El-Nahass, A. Farid and A. Atta, Structural and optical properties of Tris (8-hydroxyquinoline) aluminum (III)(Alq3) thermal evaporated thin films, *J. Alloys Compd.*, 2010, **507**(1), 112–119.
122 D. M. Mamand, *et al.*, Advanced spectroscopic approach for exploring the structural, optical, and electronic properties in dye-functionalized chitosan biopolymers, *Spectrochim. Acta, Part A*, 2025, **329**, 125485.
123 L. Li, *et al.*, First principles calculations of electronic band structure and optical properties of Cr-doped ZnO, *J. Phys. Chem. C*, 2009, **113**(19), 8460–8464.
124 X.-Y. Zhao, *et al.*, First-principles calculations of the structural, electronic and optical properties of BaZrxTi1−xO3 (x= 0, 0.25, 0.5, 0.75), *Chin. Phys. Lett.*, 2011, **28**(6), 067101.
125 S. B. Aziz, *et al.*, New Method for the Development of Plasmonic Metal-Semiconductor Interface Layer: Polymer Composites with Reduced Energy Band Gap, *J. Nanomater.*, 2017, **2017**(1), 8140693.
126 S. B. Aziz, M. A. Rasheed and H. M. Ahmed, Synthesis of polymer nanocomposites based on [methyl cellulose](1−x):(CuS) x (0.02 M≤ x≤ 0.08 M) with desired optical band gaps, *Polymers*, 2017, **9**(6), 194.
127 M. Wu, *et al.*, Al-doped ZnO monolayer as a promising transparent electrode material: a first-principles study, *Materials*, 2017, **10**(4), 359.
128 S. B. Aziz, O. G. Abdullah and M. A. Rasheed, A novel polymer composite with a small optical band gap: New approaches for photonics and optoelectronics, *J. Appl. Polym. Sci.*, 2017, **134**(21), 44847.
129 O. G. Abdullah, *et al.*, Reducing the optical band gap of polyvinyl alcohol (PVA) based nanocomposite, *J. Mater. Sci.: Mater. Electron.*, 2015, **26**, 5303–5309.
130 J. Rozra, *et al.*, Cu nanoparticles induced structural, optical and electrical modification in PVA, *Mater. Chem. Phys.*, 2012, **134**(2–3), 1121–1126.
131 M. Abdelaziz, Cerium (III) doping effects on optical and thermal properties of PVA films, *Phys. B*, 2011, **406**(6–7), 1300–1307.
132 A. S. Hassanien, A. A. Akl and I. El Radaf, *Comparative studies for determining the optical Band-gap energy of the novel polycrystalline thin Znga2s4 films sprayed at different film thicknesses*, Research Square, 2021, DOI: **10.21203/rs.3.rs-325892/v1**.
133 L. Escobar-Alarcón, *et al.*, An alternative procedure for the determination of the optical band gap and thickness of amorphous carbon nitride thin films, *Appl. Surf. Sci.*, 2007, **254**(1), 412–415.
134 D. Souri and Z. E. Tahan, A new method for the determination of optical band gap and the nature of optical transitions in semiconductors, *Appl. Phys. B*, 2015, **119**(2), 273–279.
135 D. Souri and K. Shomalian, Band gap determination by absorption spectrum fitting method (ASF) and structural properties of different compositions of (60−x) V2O5–40TeO2–xSb2O3 glasses, *J. Non-Cryst. Solids*, 2009, **355**(31–33), 1597–1601.
136 F. Ali, Structural and optical characterization of [(PVA: PVP)-Cu2+] composite films for promising semiconducting polymer devices, *J. Mol. Struct.*, 2019, **1189**, 352–359.
137 S. Thakur, *et al.*, Structural, optical and thermal properties of nickel doped bismuth borate glasses, *J. Non-Cryst. Solids*, 2019, **512**, 60–71.
138 V. Thakur, *et al.*, Effect of BaTiO3 on the structural and optical properties of lithium borate glasses, *Ceram. Int.*, 2015, **41**(9), 10957–10965.
139 A. Qasem, *et al.*, Effective role of cadmium doping in controlling the linear and non-linear optical properties of non-crystalline Cd–Se–S thin films, *J. Mater. Sci.: Mater. Electron.*, 2022, **33**(4), 1953–1965.
140 V. Dalouji, *et al.*, The optical properties of aluminum-doped zinc oxide thin films (AZO): new methods for estimating gap states, *J. Supercond. Novel Magn.*, 2019, **32**, 1319–1326.
141 S. Prasher, M. Kumar and S. Singh, Electrical and optical properties of O6+ ion beam–irradiated polymers, *Int. J. Polym. Anal. Charact.*, 2014, **19**(3), 204–211.
142 G. Attia and M. Abd El-kader, Structural, optical and thermal characterization of PVA/2HEC polyblend films, *Int. J. Electrochem. Sci.*, 2013, **8**(4), 5672–5687.
143 O. G. Abdullah, D. A. Tahir and K. Kadir, Optical and structural investigation of synthesized PVA/PbS nanocomposites, *J. Mater. Sci.: Mater. Electron.*, 2015, **26**, 6939–6944.
144 P. N. Rao, *et al.*, Optical studies of AgI–Ag2SO4–TeO2–B2O3 glass system, *Mater. Today: Proc.*, 2018, **5**(13), 26329–26338.
145 A. Dahshan, New amorphous As–Se–Sb–Cu thin films: theoretical characterization and evaluation of optical constants, *Appl. Phys. A*, 2017, **123**, 1–6.
146 A. S. Hassanien, I. El Radaf and A. A. Akl, Physical and optical studies of the novel non-crystalline CuxGe20-xSe40Te40 bulk glasses and thin films, *J. Alloys Compd.*, 2020, **849**, 156718.
147 I. Studenyak, M. Kranjčec and M. Kurik, Urbach rule in solid state physics, *Int. J. Opt. Appl.*, 2014, **4**(1), 96–104.
148 A. S. Hassanien and A. A. Akl, Effect of Se addition on optical and electrical properties of chalcogenide CdSSe thin films, *Superlattices Microstruct.*, 2016, **89**, 153–169.